ACS Catalysis

pubs.acs.org/acscatalysis Research Article

Alkene Epoxidations with H_2O_2 over Groups 4–6 Metal-Substituted BEA Zeolites: Reactive Intermediates, Reaction Pathways, and Linear Free-Energy Relationships

E. Zeynep Ayla, David S. Potts, Daniel T. Bregante, and David W. Flaherty*

Cite This: *ACS Catal.* 2021, 11, 139–154 Read Online

ACCESS | Metrics & More | Article Recommendations | Supporting Information

ABSTRACT: Rates and selectivities for alkene epoxidations depend sensitively on the identity of the active metal center for both heterogeneous and homogeneous catalysts. While group 6 metals (Mo, W) have greater electronegativities and the corresponding molecular complexes have greater rates for epoxidations than group 4 or 5 metals and molecular complexes, these relationships are not established for zeolite catalysts. Here, we combine complementary experimental methods to determine the effects of metal identity on the catalytic epoxidation of 1-hexene with H_2O_2 for active sites within the BEA framework. Postsynthetic methods were used to incorporate groups 4–6 transition-metal atoms (Ti, Nb, Mo, W) into the framework of zeolite BEA. *In situ* Raman and UV–vis spectroscopies show that H_2O_2 activates to form peroxides (M-(η^2-O_2)) and hydroperoxides (M-OOH) on all M-BEA but also metal oxos (M═O) on W- and Mo-BEAs, the latter of which leaches rapidly. Changes in turnover rates for epoxidation as functions of reactant concentrations and the conformation of *cis*-stilbene epoxidation products indicate that epoxide products form by kinetically relevant O-atom transfer from M-OOH or M-(η^2-O_2) intermediates to the C═C bond and show two distinct kinetic regimes where H_2O_2-derived intermediates or adsorbed epoxide molecules prevail on active sites. Ti-BEA catalyzes epoxidations with turnover rates 60 and 250 times greater than Nb-BEA and W-BEA, which reflect apparent activation enthalpies ($\Delta H^{\ddagger}$) for both epoxidation and H_2O_2 decomposition that are lower for Ti-BEA than for Nb- and W-BEAs. Values of $\Delta H^{\ddagger}$ for epoxidation differ much more between metals than barriers for H_2O_2 decomposition and give rise to large differences in 1-hexene epoxidation selectivities that range from 93% on Ti-BEA to 20% on W-BEA. Values of $\Delta H^{\ddagger}$ for both pathways scale linearly with measured enthalpies for adsorption of 1,2-epoxyhexane from the solvent to active sites measured by isothermal titration calorimetry. These correlations confirm that linear free-energy relationships hold for these systems, despite differences in the coordination of active metal atoms to the BEA framework, the identity and number of pendant oxygen species, and the complicating presence of solvent molecules.

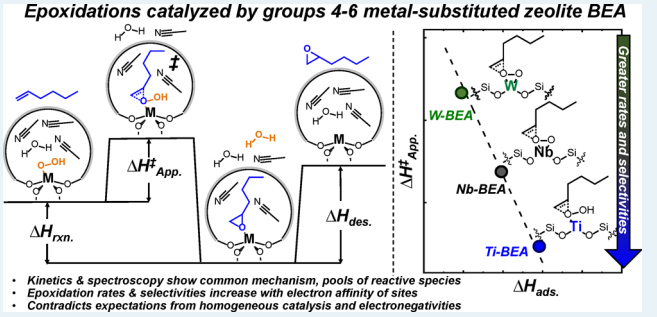

KEYWORDS: *titanium, niobium, molybdenum, tungsten, in situ spectroscopy, Raman spectroscopy, active site titrations*

1. INTRODUCTION

Epoxides are important precursors for the production of performance solvents, solutions, materials, and biologically active ingredients within the food, cosmetic, construction, automobile, and pharmaceutical industries.[1] The synthesis and characterization of a catalyst comprised of titanium substituted into the framework of MFI zeolite (i.e., titanium-silicate-1, TS-1) by ENI in 1983 gave rise to the use of hydrogen peroxide (H_2O_2) as an environmentally benign alternative to chlorine and organic hydroperoxides for the production of propylene oxide. The success of this system continues to motivate the development of new transition-metal-silicate catalysts,[2−7] integrated processes,[8−10] and investigations of fundamental surface chemistry for the epoxidation of alkenes with H_2O_2.[5,11,12] Recent finding show that rates and selectivities for epoxidations with H_2O_2 depend strongly upon the identity of the active transition metal[4,13] and the topology, pore size, and the silanol density of the silicate support.[2,11,14] These attributes influence the form and electronic structure of H_2O_2-derived intermediates and solvent-mediated interactions among reactive species and the extended surface of the silicate support.

Early transition metals activate H_2O_2 for epoxidations.[15] Groups 4 and 5 metals (Ti, Nb, Ta) grafted onto mesoporous

Received: August 3, 2020
Revised: November 20, 2020

https://dx.doi.org/10.1021/acscatal.0c03394
ACS Catal. 2021, 11, 139–154

supports,[3,12,16,17] incorporated into zeolite frameworks[6,7,13,18] or as polyoxometalates (POMs),[19−22] have been widely studied to examine the effects of active metal identity on epoxidation catalysis over solid materials. The electron affinity of the active metal atom likely impacts catalysis by influencing the electrophilicity of reactive forms of oxygen bound to active sites. In agreement with intuition, the electronic properties of active sites for these catalysts depend strongly on those of the associated transition metals and influence activation enthalpies for epoxidation. Multiple studies have shown that more electrophilic reactive intermediates epoxidize alkenes with greater turnover rates.[4,13,23] Ti, Nb, Ta, Zr, and Hf in framework sites of zeolite BEA all form metal-peroxo (M-(η^2-O_2)) and metal-hydroperoxo (M-OOH) structures from H_2O_2; however, turnover rates for epoxidation are as much as 5000-, 100-, and 50-fold higher on Ti-based catalysts than on analogous Zr- or Hf-, Ta-, and Nb-based catalysts, respectively.[3,13] The ligand-to-metal charge transfer (LMCT) energies of these reactive intermediates serve as a quantitative measure of the electrophilicity of reactive oxygen species and can be determined by *in situ* UV−vis spectroscopy. For both amorphous silicates and crystalline zeolite BEA, the apparent activation enthalpies ($\Delta H^{\ddagger}$) for alkene epoxidation and H_2O_2 decomposition correlate linearly with the LMCT energies of reactive intermediates and also with the enthalpies of adsorption for gaseous basic probe molecules (e.g., pyridine or deuterated acetonitrile) onto the Lewis acidic active sites.[3,13] Kholdeeva et al. examined cyclooctene epoxidation on Ti- and Nb-silicates,[17,24] and Carbó and co-workers studied reactions of H_2O_2 and cyclohexene over Ti- and Nb-atoms grafted to tungsten-based Lindqvist polyoxometallates (POM).[21,22] These reports proposed that both Ti and Nb active sites epoxidize alkenes via metal-hydroperoxo (M-OOH) reactive intermediates, and Nb catalysts provide lower apparent activation energies for epoxidations than the corresponding Ti-based catalysts. These differences were concluded to reflect the greater electrophilicity of the Nb active sites.[21,22,24] Overall, the strong correlation of these kinetic and thermodynamic quantities suggests that active sites with greater electron affinities (i.e., stronger Lewis acid character) provide lower $\Delta H^{\ddagger}$ and also greater rates and selectivities for alkene epoxidations among series of otherwise similar metal-silicate catalysts.

We hypothesized these trends would extend to catalytically relevant group 6 metals (e.g., Mo and W), which due to their relatively high Pauling electronegativities (2.16 and 2.36 for Mo and W compared to 1.54 and 1.6 for Ti and Nb, respectively),[25] may explain the previous reports of high rates on W- and Mo-based molecular catalysts. For example, Sheldon reports that higher redox potentials and Lewis acidity of soluble transition-metal complexes lead to increasing reactivity for epoxidation with organic hydroperoxides and ranks the reactivity of molecular metal complexes in the order of decreasing rates: Mo > W > Ti, V.[26,27] Propylene epoxidation processes employ solid Ti-silicates (e.g., Shell Styrene Monomer Propylene Oxide process with ethylbenzene hydroperoxide, Dow Hydrogen Peroxide-Propylene Oxide process) in addition to soluble Mo-complexes (e.g., Halcon process with tert-butyl hydroperoxide).[28−30] Extensive studies of molecular Mo and W catalysts suggest that reaction with H_2O_2 forms homogeneous Mimoun complexes (i.e., stable metal centers possessing both metal-oxo and metal-peroxo functions), which transfer oxygen atoms from peroxo groups to alkenes during epoxidations.[31−35] In comparison, only a few studies have examined heterogeneous group 6 metal catalysts for epoxidations.[36−42] For example, Hammond et al. reported that bulk WO_3 species are the more active form of supported W catalysts for cyclooctene epoxidation.[42] The absence of comparisons between supported groups 4−6 early transition-metal catalysts stems, in part, from the instability of Mo and W on amorphous solid supports, which allows these metals to leach into solution or polymerize on surfaces.[43,44] In addition, most investigations of supported group 6 metals use organic hydroperoxides as oxidants and fewer examine catalysis with H_2O_2.[27,45,46]

Here, we synthesize groups 4−6 metal atom (Ti, Nb, Mo, and W) substituted zeolite BEA materials with the intent to create a homologous series of catalysts that possess isolated metal active sites within pores of identical topology and polarity. We combine kinetic, spectroscopic, and calorimetric methods to determine how the identity of the reactive intermediates, the reaction pathways, and relevant kinetic barriers for the epoxidation of alkenes with H_2O_2 depend on differences in the identity of the framework-substituted transition-metal atoms. UV−vis and Raman spectroscopy together with *in situ* titrations of active sites with phosphonic acids demonstrate that selected W-, Ti-, and Nb-BEA materials predominantly stabilize monomeric active sites present at tetrahedral sites likely within the BEA framework. However, Mo leaches rapidly from the framework that the stable M-BEA (M = Ti, Nb, W) catalysts mediate epoxidations by equivalent series of elementary steps that are described with a single-rate expression. Analysis of the products of *cis*-stilbene epoxidation and *in situ* Raman and UV−vis spectra gives evidence that Ti-OOH, Nb-(η^2-O_2), and W-(η^2-O_2) are the reactive intermediates for epoxidation on each of the respective metal atoms. Turnover rates and selectivities for 1-hexene epoxidation are lower for W-BEA despite expectations that W's greater Pauling electronegativity would give rise to much higher rates. Consistent with these differences, $\Delta H^{\ddagger}$ for epoxidation on W-BEA exceeds those for Ti- and Nb-BEA by more than 30 kJ mol^{-1} at equivalent coverages of reactive intermediates. Despite these deviations from expectations, the differences among $\Delta H^{\ddagger}$ values correlate with enthalpies for liquid-phase adsorption of 1,2-epoxyhexane, as measured by isothermal titration calorimetry (ITC). These comparisons confirm that group 4−6 active metal sites in the BEA framework follow classical linear free-energy relationships and show that comparisons of electronegativities of individual elements do not provide accurate predictions for the electronic properties of active sites in these zeolite catalysts. These distinctions likely reflect variations in framework coordination and pendant functions (e.g., hydroxyl, oxo groups) among these active sites.

2. MATERIALS AND METHODS

2.1. Catalyst Synthesis. M-BEA catalysts, where M refers to the identity of the metal incorporated into the zeolite (M = Ti, Nb, Mo, W), were synthesized by postsynthetic modification of commercial Al-BEA samples. Al-BEA (TOSOH, lot no. 94HA6X02Y; Si:Al = 20) was refluxed in HNO_3 (Macron Chemicals, 68−70 wt %; Caution: HNO_3 can cause severe chemical burns and should be handled with care) to remove Al atoms from the BEA framework, likely by forming soluble $Al(NO_3)$ species that traverse pores and enter the bulk liquid. The dealuminated BEA was recovered by

https://dx.doi.org/10.1021/acscatal.0c03394
ACS Catal. 2021, 11, 139−154

vacuum filtration and washed with H_2O (17.5 MΩ cm, 60 cm^3 g^{-1}). These samples were then heated to 823 K (4 K min^{-1}) in flowing dry air (100 cm^3 min^{-1}; Airgas, Ultra Zero grade) and held at 823 K for 6 h to desorb or oxidize residues (e.g., water, organics) remaining after the synthesis and dealumination processes. Subsequent characterizations by energy- dispersive X-ray fluorescence (EDXRF) and X-ray diffraction (XRD) show that these treatments remove nearly all Al, leaving only trace quantities (Si:Al > 2400) but leave the crystalline BEA framework intact.

Transition-metal atoms were incorporated into tetrahedral vacancies in the BEA framework by adsorption of metal chlorides within appropriate polar solvents, using a methodology similar to our prior reports for Ti-, Nb-, and Ta-BEA catalysts.[3,13] The dealuminated BEA (Si-BEA) was loaded into a round-bottom flask heated under vacuum (<5 Pa, 473 K) for 2 h to remove free water molecules. The moisture-free solids are suspended in a solvent (dichloromethane, Fisher Chemicals, 20 cm^3 $g_{zeolite}^{-1}$) for Ti-BEA and Mo-BEA, isopropyl alcohol (Fisher Chemicals, 20 cm^3 $g_{zeolite}^{-1}$) for Nb-BEA, and chloroform (Fisher Chemicals, 20 cm^3 $g_{zeolite}^{-1}$) for W-BEA. Schlenk methods are used to introduce $TiCl_4$ (Sigma Aldrich, ≥99.0%), $MoCl_5$ (Sigma Aldrich, 99.99% trace metals basis (excluding W)), $NbCl_5$ (Sigma Aldrich, 99%), or WCl_6 (Sigma Aldrich, ≥99.9% trace metals basis) to the mixture of solvent and Si-BEA. The resulting mixture is heated to reflux under flowing Ar (Airgas, Ultra zero grade) and stirred (350 rotations per minute (rpm)) for 8 h with the intent to dissociatively bind the metal chloride at silanol nests ($(SiOH)_4$) generated by the dealumination treatment. The solutions of metal chlorides and Si-BEA are initially colored distinctly ($TiCl_4$ is white; $MoCl_5$ is orange; WCl_6 is dark green; and $NbCl_5$ is colorless), however, the solutions all became white and opaque after ∼8 h as a result of the reactive adsorption of the metal complexes to the Si-BEA support. The solids were recovered by rotary evaporation (IKA, RV 10) and were heated at 5 K min^{-1} in flowing dry air (100 cm^3 min^{-1}) and held at 823 K for 6 h. Following this oxidative treatment, the M-BEA samples appear as white powders.

2.2. Catalyst Characterization. The elemental compositions of the M-BEA samples were determined by EDXRF. Finely ground samples of M-BEA (∼50 mg) were placed in a 1 cm-diameter sample holder, sealed with an ultralene film, and loaded into the He-purged chamber of the spectrometer (Shimadzu, EDX-7000). The sample was scanned between 0 and 30 keV and the elemental composition of the sample was calculated using the relative intensities of the corresponding fluorescence peaks.

The dispersities of the Ti, Nb, Mo, and W atoms present on the M-BEA materials were examined with diffuse reflectance UV-Vis (DRUV-vis) spectroscopy to measure metal band gap energies using a UV-vis spectrophotometer (Varian Cary 5G). M-BEA samples were intimately mixed and ground with magnesium oxide (MgO; Sigma Aldrich, 99.995%) at a MgO to M-BEA mass ratio of 10:1, and pure MgO was used to obtain background spectra. Band gap energies were determined by extrapolating the linear portion of the Tauc plots to the horizontal axis representing photon energy (eV) (Figure S1). Figure 1 shows Tauc plots (i.e., Kubelka−Munk (K−M) absorbances as a function of photon energy) for W-BEA samples with W contents ranging from 0.12 to 1.7 W atoms per unit cell (0.55−7.8 wt%). These samples possess band gaps that decrease systematically (3.85−4.41 eV) with increasing

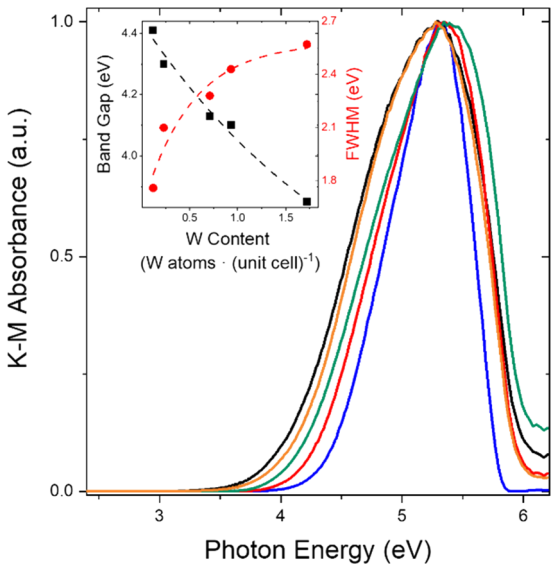

Figure 1. Tauc plots of W-BEA (0.12 (blue line), 0.23 (red line), 0.71 (green line), 0.93 (orange line), and 1.72 (black line) W atoms per unit cell) derived from DRUV-vis spectra under ambient conditions were used to plot (inset) the band gap and FWHM of DRUV-vis absorbance feature as functions of the tungsten content (W atoms (unit cell)$^{-1}$).

metal content and that are greater than the band gap for bulk WO_3 (2.8 eV),[47] which indicates that the W atoms in these samples are relatively disperse. Both the band gap energies and the widths of the absorbance features change asymptotically with decreasing W atom loading (Figure 1, inset) suggesting that the distribution of W complexes becomes increasingly uniform and contains greater fractions of monomeric species.[48] We therefore maximize the fraction of isolated W atoms by use of low metal loadings during post-synthetic modification.[49,50] We have previously reported synthesis and characterization of comparable Ti- and Nb-BEA materials.[3,13,51]

The crystallinities of the M-BEA samples were determined using an X-ray diffractometer (Siemens-Bruker, D5000) with Cu Kα radiation under ambient conditions. The diffractograms obtained (Figure S2) match reported powder diffraction patterns for zeolite BEA without observable changes in peak positions for the specific metal contents reported in Table 1. Higher metal loadings (> 0.95 atoms (unit cell)-1) of Ti, Nb, and Ta, however, shift diffraction features to lower angles due to a slight expansion of the unit cell.[51] W loadings greater than

Table 1. Metal Loading, Metal Atoms per Unit Cell, Band Gap, and Percentage of Active Metal for M-BEA Samples Used in Catalytic Measurements

catalyst	metal loading (wt %)[a]	metal atoms per unit cell	band gap (eV)[b]	bulk metal oxide band gap (eV)	active metal (%)[c]
Ti-BEA	0.25	0.20	4.34	3.2	100 ± 4
Nb-BEA	0.22	0.09	4.73	3.4	100 ± 6
W-BEA	1.1	0.23	4.30	2.8	70 ± 5
Mo-BEA	0.4	0.16	3.96	2.9	n.d.[d]

[a]Measured by EDXRF (section 2.2), [b]Determined by DRUV-vis (section 2.2, Figure S1), [c]Calculated from *in situ tert*-butyl phosphonic acid titrations (section 2.3, Figure S8), [d]Not determined; leaching of Mo from BEA framework during catalysis precluded attempts to titrate number of active sites.

https://dx.doi.org/10.1021/acscatal.0c03394
ACS Catal. 2021, 11, 139−154

1.7 atoms (unit cell)$^{-1}$ show a similar change. These results show all M-BEA retain the BEA framework structure after dealumination and metal incorporation.

Table 1 displays the metal content of the M-BEA samples used for catalytic rate measurements, *in situ* UV−vis experiments, and isothermal titration calorimetry. These samples contain low transition-metal contents (<0.25 atoms (unit cell)$^{-1}$, on average) to form monomeric species within the BEA framework, avoid internal mass transfer constraints,[47] and present active sites in intrapore environments with similar silanol densities.[14] M-BEA samples with greater densities of transition metal atoms were used for *ex situ* characterization and for *in situ* Raman experiments to examine changes in physical properties with the metal content and to identify spectroscopic features related to monomeric and oligomeric species.

2.3. Epoxidation and H_2O_2 Decomposition Turnover Rate Measurements. Turnover rates for 1-hexene (C_6H_{12}) epoxidation with H_2O_2 on M-BEA were measured in liquid CH_3CN, at low temperatures (303−333 K), and in stirred batch reactors (700 rpm) at differential conversion (<0.5%). These conditions avoid internal mass transfer constraints at turnover rates, particle sizes, and site densities used in this study, as we have shown using the Madon−Boudart criterion.[3,13] The alkene substrate, decane (an internal standard), and H_2O_2 were stirred in CH_3CN at 313 K, and an initial aliquot (~0.5 cm^3) was taken after 30 min. After the addition of ~10−50 mg of catalyst, aliquots were taken at regular intervals using a syringe equipped with a polypropylene filter (Tisch Scientific, 0.05 μm) to separate the catalyst particles from the sample and halt the reaction. Products were analyzed with a gas chromatograph (Agilent, 6850) equipped with a flame ionization detector and liquid autosampler (CTC Analytics, GC Pal). Comparisons between replicated rate measurements indicate that the experimental uncertainty of these measurements is ~10%.

Hot filtration tests were used to determine if metal atoms leach from the BEA zeolite and form soluble complexes active for epoxidation. During a batch reaction, an aliquot of the mixture (~10 mL) was taken at 10 min, filtered (0.05 μm), and transferred into a stirred and heated 20 cm^3 scintillation vial (700 rpm, 313 K). Subsequently, aliquots were taken from the scintillation vial as a function of time and the concentrations of all species were determined by gas chromatography. Hot filtered solutions taken from reactions with Ti-BEA, Nb-BEA, and W-BEA did not show any change in epoxide concentration following filtrations. Hot filtered solutions taken from reactions with Mo-BEA did, however, show measurable increases in the concentration of epoxide, which indicates this sample produces soluble metal complexes active for epoxidation.

Hydrogen peroxide decomposition rates were measured using colorimetric titration with an aqueous titrant solution of $CuSO_4(H_2O)_5$ (8.3 mM; VWR, 99%) and neocuproine hydrate (12 mM; SAGECHEM) in an aqueous solution of ethanol (4.3 M; Decon Laboratories, 100%). The reaction solution (0.15 cm^3) was titrated with a combination of titrant (1 cm^3) and DI H_2O (0.85 cm^3), and the absorbance at 454 nm was determined using a UV−vis spectrophotometer (Spectronic, 20 Genesys). The corresponding H_2O_2 concentration values were used to calculate H_2O_2 decomposition rates by subtracting the formation rate of 1,2-epoxyhexane from the total rate of H_2O_2 consumption.

Catalytically active sites were titrated *in situ* with phosphonic acids (PA) to determine the fraction of metal atoms that contribute to measured epoxidation rates.[3,48] *tert*-Butyl phosphonic acid (TBPA; Sigma Aldrich, 98%) or methyl phosphonic acid (MPA; Sigma Aldrich, 98%), 1-hexene, decane, and the catalyst were combined with CH_3CN in the reaction flask and stirred for 30 min (700 rpm, 313 K) to allow the PA to bind to M atoms. H_2O_2 was then added to initiate the reaction, and aliquots were taken and analyzed as before. These experiments were conducted for multiple ratios of [PA] to [M] with values ranging from 0 to 2 to determine how apparent turnover rates decrease as a function of the amount of titrant. The number of catalytically active sites within each sample was calculated by a linear fit of the titration results at the lowest coverages and with the assumption that each PA molecule binds to one metal center. Analysis of these results (section 3.2) shows that *in situ* titrations with TBPA provide a more accurate estimate for site counts than titrations with MPA (see below). Consequently, the percentages of active metal atoms in Table 1 are determined from titrations with TBPA.

2.4. *In Situ* Raman and UV−vis Spectroscopy. *In situ* Raman and UV−vis spectra of species formed by the activation of H_2O_2 on M-BEA samples were obtained by placing catalyst pellets (30−50 mg) in a custom-built liquid flow cell. Steady-state spectra of the H_2O_2-derived surface species were collected in a solution of H_2O_2 (10 mM H_2O_2, 39 mM H_2O, 313 K) in flowing CH_3CN, introduced at 1 cm^3 min^{-1} by an HPLC pump (SSI, LS Class).

H_2O_2 activation on M-BEA was observed using a Raman spectrometer (Renishaw, InVia) equipped with a 442 nm laser that delivered a power density of 0.8 mW μm^{-2} at the sample, as measured directly by a power meter (Gentec-EO, PRONTO-Sl). Reported spectra were obtained with a long 50X objective and represent the average of 100 scans (10 scans s^{-1}) at an estimated resolution of 2 cm^{-1}. To increase Raman peak intensity and clearly observe features unique to H_2O_2 activation, we used M-BEA synthesized with high metal content (1.2 wt % Ti, 3 wt % Nb, 5 wt % W, 5 wt % Mo). Intermediates formed upon *in situ* H_2O_2 activation were also examined using a fiber-optic UV−vis spectrometer (Avantes, AvaFast 2048). Absorbance features were deconvoluted by performing baseline subtraction and Gaussian peak fittings using OriginPro software.

2.5. Isothermal Titration Calorimetry on M-BEA Catalysts. Enthalpies for adsorption of 1,2-epoxyhexane onto M-BEA catalysts were determined using an isothermal titration calorimeter (TA Instruments, NanoITC) equipped with both reference and sample cells. A solution of 1,2-epoxyhexane (10 mM $C_6H_{12}O$; Sigma-Aldrich, 97%) in CH_3CN (39 mM H_2O) was used to titrate a slurry of ~20−30 mg of M-BEA in CH_3CN (39 mM H_2O, 313 K, 250 rpm). Values of 1,2-epoxyhexane adsorption enthalpies were determined by averaging heats released upon titration of M-BEA at substoichiometric (<0.2) quantities of 1,2-epoxyhexane relative to metal sites in M-BEA with the assumption that all titrant molecules adsorb to M atoms.

3. RESULTS AND DISCUSSION

3.1. Reactive Species Formed upon H_2O_2 Activation. Early transition-metal atoms (Ti, Nb, W, and Mo) substituted in BEA activate H_2O_2 to form pools of surface intermediates, including metal peroxide (M-(η^2-O_2)),[33] metal hydroperoxide

https://dx.doi.org/10.1021/acscatal.0c03394
ACS Catal. 2021, 11, 139−154

(M−OOH),[3,13] and metal oxo (M═O)[49] species that have been implicated in liquid-phase oxidation reactions. Here, we combine *in situ* Raman and UV−vis spectroscopies with analysis of product distributions from *cis*-stilbene epoxidation to determine the identities of reactive species that directly transfer oxygen atoms to alkenes during epoxidation. Figure 2

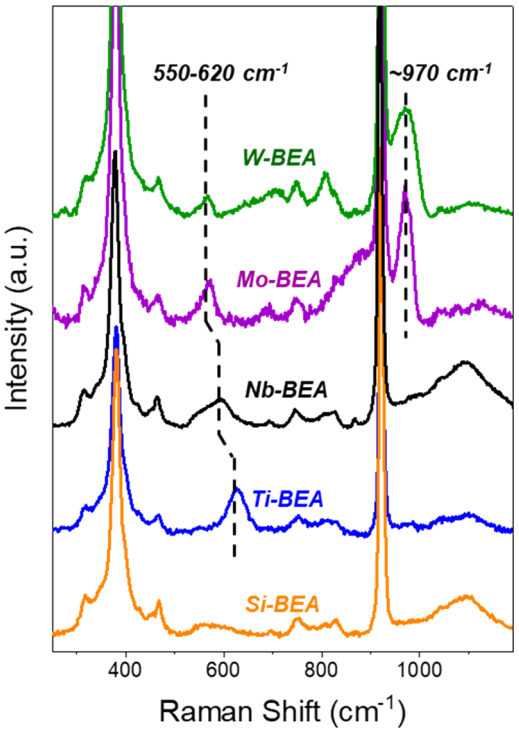

Figure 2. *In situ* Raman spectra (442 nm laser, 0.8 mW·μm^{-2}) in flowing CH_3CN (10 mM H_2O_2, 39 mM H_2O, 313 K, 1 cm^3 min^{-1}). Spectra are offset and normalized to a feature of the BEA framework at 312 cm^{-1}. The spectrum for Mo-BEA is obtained ∼100 s after contact with the H_2O_2 solution, and all others are taken at steady-state.

shows steady-state Raman spectra of Si-, Ti-, Nb-, W-, and Mo-BEA within flowing solutions of H_2O_2 (10 mM H_2O_2, 39 mM H_2O, in CH_3CN, 313 K). All spectra are normalized to vibration of the BEA zeolite framework at 312 cm^{-1}[50] to facilitate comparisons among materials, and spectra include large features associated with the CH_3CN solvent at 375 cm^{-1} and 920 cm^{-1}.[51] In addition, all spectra of M-BEA samples contain features at 694 cm^{-1} and from 750 to 825 cm^{-1}, which correspond to framework vibrations of zeolite BEA[52] and appear in *ex situ* spectra (Figure S3).

The Raman spectra of H_2O_2-activated Ti-, Nb-, Mo-, and W-BEA contain features between 550 and 620 cm^{-1} that correspond to the symmetric and asymmetric stretching modes of metal-peroxo (M-(η^2-O_2)) intermediates.[53−56] The position of ν(M-(η^2-O_2)) shifts to lower wavenumbers from Ti-BEA[53] to Nb-BEA, Mo-BEA, and W-BEA[54] due to greater charge transfer from the group 6 metal center to the peroxide moiety.[57] In addition to features that appear only after contact with H_2O_2, spectra for Mo- and W-BEA possess a distinct feature near 970 cm^{-1} (Figure 2), which is attributed to ν(M═O)[58,59] and is absent from spectra of Ti-BEA and Nb-BEA. Mo-BEA and W-BEA also show Raman features reminiscent of oligomeric metal oxides complexes including bridging M−O−M bonds at 700 cm^{-1}[59] and 805 cm^{-1} for WO_3 and 880 cm^{-1} for MoO_3.[58−60] The vibrational features (700 and 805 cm^{-1}) that correspond to bulk WO_3 increase monotonically with W content (Figure S3), which shows that extra-framework WO_x oligomers form at higher loadings.[61] Similarly, greater loadings tend to form oligomeric MoO_x on Mo-BEA. Collectively, these Raman spectra show that all Ti-, Nb-, W-, and Mo-BEA activate H_2O_2 to form M-(η^2-O_2) species, while W- and Mo-BEA materials also possess distinguishable M═O functions.

Figure 3 shows steady-state UV−vis spectra of Ti-, Nb-, and W-BEA collected *in situ* after H_2O_2 activation (10 mM H_2O_2,

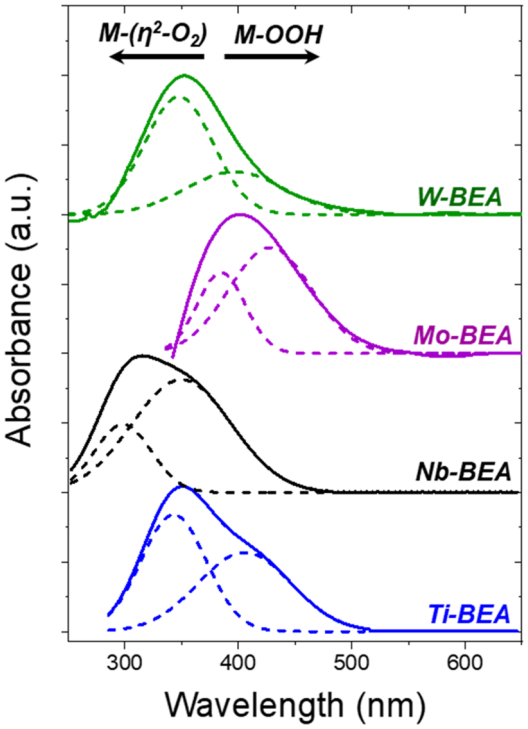

Figure 3. Difference UV−vis spectra of H_2O_2 activated Ti-BEA (blue line), Nb-BEA (black line), Mo-BEA (purple line), and W-BEA (green line) acquired *in situ* within flowing CH_3CN (10 mM H_2O_2, 39 mM H_2O, 313 K, 1 cm^3 min^{-1}). Spectra are offset and normalized by the maximum absorbance value. The background spectrum for each M-BEA was obtained in CH_3CN (39 mM H_2O, 313 K) before contact with H_2O_2.

39 mM H_2O in CH_3CN, 313 K). These spectra contain broad asymmetric features between 250 and 500 nm, which agree with reports for the ligand-to-metal charge transfer (LMCT) peaks of M-(η^2-O_2) and M-OOH species on metal atoms grafted to mesoporous SiO_2,[3,17,62] incorporated into the framework of zeolite BEA,[13] and for homogeneous complexes.[63] These interpretations agree with earlier studies that assigned the UV−vis absorbance features to the changing coordination state of Ti atoms incorporated into the zeolite framework[64,65] and more recent evidence from Tilley et al.[62,66] and Ivanchikova and co-workers[17] that indicates the observed UV features for H_2O_2-activated transition-metal centers on silica reflect the presence of both metal hydroperoxo and metal peroxo species. These UV−vis spectra (Figure 3) consist of two overlapping LMCT peaks, where the higher energy (lower wavelength) feature corresponds to M-(η^2-O_2) intermediates, and the lower energy feature signifies M-OOH species. These features were confirmed over Ti-BEA, Nb-BEA, and Ta-BEA

https://dx.doi.org/10.1021/acscatal.0c03394
ACS Catal. 2021, 11, 139−154

materials by correlating reversible changes in the relative intensities of the M-OOH and M-(η^2-O_2) features to the concentration of protons in aqueous solutions.[3]

In situ Raman and UV−vis spectra along with post-reaction EDXRF show that Ti-, Nb-, and W-BEA are stable and show little to no metal dissolution during catalysis (≤7% for W-BEA, immeasurable changes for Ti- and Nb-BEA after 2 h in CH_3CN (10 mM H_2O_2, 39 mM H_2O, 313 K, 700 rpm)); however, molybdenum atoms leach rapidly from the BEA framework following contact with H_2O_2. Time-resolved Raman (Figure S4) and UV−vis spectra (Figure S6) collected *in situ* show that vibrational features and LMCT bands specific to Mo-containing complexes completely attenuate after 0.5−2.5 h of contact with H_2O_2 in CH_3CN (10 mM H_2O_2, 39 mM H_2O, 313 K), and EDXRF indicates at least 90% loss of Mo from BEA. Consequently, further comparisons among M-BEA catalysts omit Mo-BEA.

Scheme 1 displays plausible structures for reactive M-OOH and M-(η^2-O_2) intermediates detected by *in situ* Raman

Scheme 1. Proposed Structure of H_2O_2-Derived Intermediates on Groups 4−6 Metals in Zeolite BEA. Solvent Molecules Have Been Omitted for Clarity

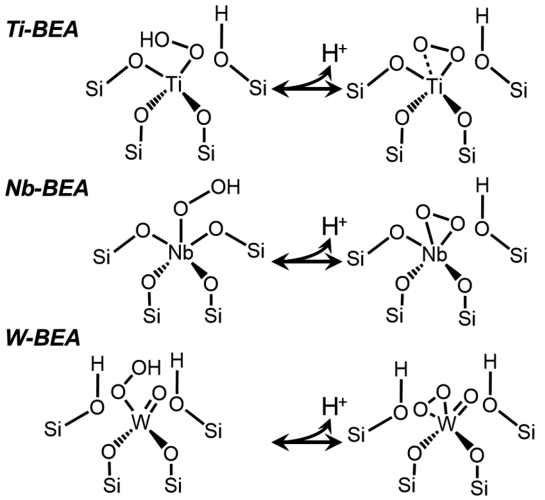

(Figure 2) and UV−Vis spectra (Figure 3) of M-BEA catalysts in contact with H_2O_2. Titanium and niobium ions substituted into zeolites commonly acquire four framework bonds (e.g., as $Ti(OSi)_4$[67] or $Nb(OSi)_4OH$[68]) and activate H_2O_2 to form M-OOH and M-(η^2-O_2) species.[68,69] The coordination of metal hydroperoxo species (M-(η^2-OOH) or M-(η^1-OOH)) for metal silicates remains under debate.[24,62] Detailed characterization of Mo[70−72] and W[73−75] atoms grafted to silica surfaces by X-ray absorption spectroscopy, infrared spectroscopy, and ^{29}Si nuclear magnetic resonance suggest these atoms may adopt bipodal surface coordination with M═O ligands under hydrated and dehydrated conditions. Density functional theory predicts that the predominant coordination structure of group 6 metal atoms at the framework position in BEA possesses two framework bonds with remaining coordination to metal-dioxo ligands (i.e., $M(OSi)_2O_2$) in the presence of water; however, the precise coordination structure has not yet been confirmed experimentally.[76] With these expectations, we tentatively interpret the Raman spectra in Figure 2 to suggest that $W(OSi)_2O_2$ moieties activate H_2O_2 to form W-(η^2-O_2) and W-OOH species that bind together with oxo ligands (e.g., as $W(OSi)_2(\eta^2\text{-}O_2)O$), as depicted in Scheme 1. We depict the coordination of the W-atom based upon recent reports for W on silica surfaces,[77] although other coordination structures with three or four linkages to the BEA framework may exist.

Prior literature establishes that one complex within these pools of reactive intermediates on a given metal center dominates rates for oxygen transfer to alkenes within epoxidation reactions.[13,78] The most significant reactive intermediate for epoxidation on Ti and Nb atoms substituted into BEA[3,13] or supported on amorphous silica[3] are Ti-OOH and Nb-(η^2-O_2), respectively. While there are fewer studies for heterogeneous W materials,[79,80] catalytic investigations of molecular complexes of group 6 metals suggest that W-(η^2-O_2) is the reactive intermediate for epoxidations.[31−33] *In situ* Raman spectra show no observable changes in the feature corresponding to W═O complexes (970 cm^{-1}) when 1-hexene contacts W-BEA in the absence of H_2O_2, and no detectable amounts of 1,2-epoxyhexane form over 1 h at 313 K. Therefore, the oxo functions do not transfer O-atoms to alkenes at conditions used in this investigation. Consequently, M-OOH and M-(η^2-O_2) are the remaining plausible reactive intermediates for epoxidation over W-BEA.

Analysis of the distribution of isomers formed during the epoxidation of *cis*-stilbene with H_2O_2 over W-BEA (and Ti- and Nb-BEA) catalysts provide evidence for the identity of the surface intermediate responsible for epoxidation on each material. Epoxidation reactions with M-OOH and M═O species both occur through a concerted oxidation mechanism that inhibits stereochemical rearrangement[81,82] and forms *cis*-stilbene epoxide as the dominant product. In contrast, M-(η^2-O_2) functions react with alkenes through a stepwise mechanism that involves the formation of a radical M-OO· moiety and sequential formation of C−O bonds, which allows for C−C bond rotation and isomerization.[28,83,84] Consequently, reactions with M-(η^2-O_2) moieties yield comparable concentrations of *cis*- and *trans*-stilbene oxide. Table 2 shows

Table 2. Products of *cis*-Stilbene Epoxidation with H_2O_2, Reactive Oxygen Species, and Corresponding LMCT Energies

catalyst	ratio of *cis*- to *trans*-stilbene oxide[a]	reactive intermediate for epoxidation[b]	LMCT energy of reactive intermediate (eV)[c]
Ti-BEA	2.6 ± 0.1	Ti-OOH	3.1
Nb-BEA	0.9 ± 0.1	Nb-(η^2-O_2)	4.2
W-BEA	0.7 ± 0.1	W-(η^2-O_2)	3.6
Mo-BEA	n.d.[d]	Mo-(η^2-O_2)[e]	3.2

[a]Ratio of turnover rates for *cis*-stilbene epoxide and *trans*-stilbene epoxide measured with 20 mM *cis*-stilbene, 10 mM H_2O_2, and 39 mM H_2O in CH_3CN at 313 K. [b]Determined from the ratio of *cis*- to *trans*-stilbene oxide. [c]Determined by deconvolution of UV−vis spectra measured *in situ* in CH_3CN (10 mM H_2O_2, 39 mM H_2O, 313 K, 1 mL min^{-1}) over M-BEA. [d]Not determined; leaching of Mo from the BEA framework during catalysis-precluded attempts to measure *cis*-stilbene epoxidation rates. [e]An extension of results for W-BEA and prior studies for Mo-complexes (Mo-(η^2-O_2)).[33]

the distributions of product isomers from *cis*-stilbene epoxidation with H_2O_2 over each M-BEA, which were determined by measured concentration profiles as functions of time (Figure S7). Ti-BEA forms primarily *cis*-stilbene oxide, whereas Nb-BEA and W-BEA form similar quantities of *cis*- and *trans*-stilbene oxides. These results indicate that Ti-BEA

https://dx.doi.org/10.1021/acscatal.0c03394
ACS Catal. 2021, 11, 139−154

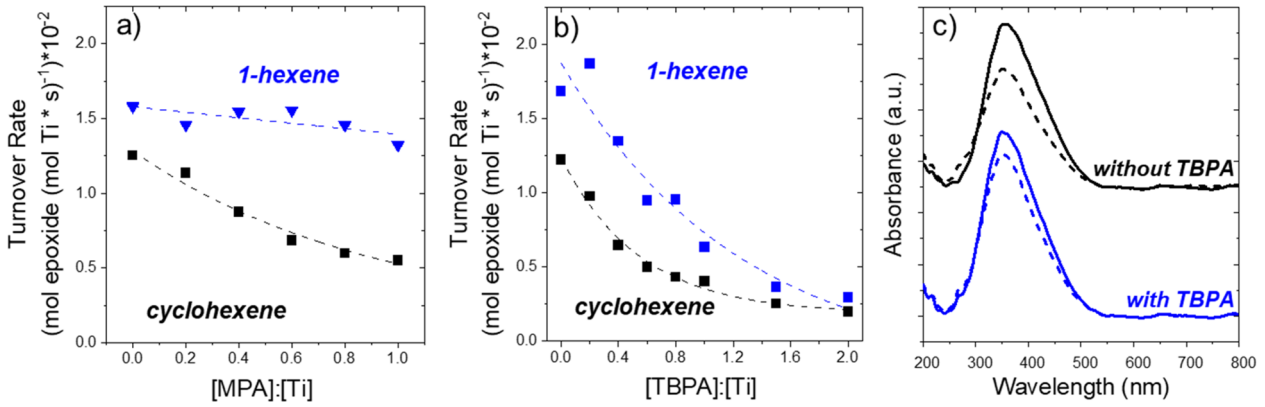

Figure 4. Turnover rates for cyclohexene and 1-hexene epoxidation with H_2O_2 over Ti-BEA as a function of (a) methyl phosphonic acid (MPA) to incorporated Ti ratio and (b) *tert*-butylphosphonic acid (TBPA) to incorporated Ti ratio. (c) UV−vis spectra of Ti-BEA collected *in situ* first in CH_3CN (10 mM H_2O_2, solid) and then CH_3CN (0.1 M C_6H_{12}, dashed) with (blue) and without (black) the addition of TBPA prior to contact with the H_2O_2 solution.

reacts through Ti-OOH, and Nb-BEA and W-BEA react through Nb-(η^2-O_2) and W-(η^2-O_2) species, respectively.

The electronic properties of reactive M-OOH and M-(η^2-O_2) species affect the activation barriers for O-atom transfer during epoxidations. Table 2 lists the LMCT energies for the reactive M-OOH and M-(η^2-O_2) intermediates on Ti-, Nb-, and W-BEA observed in Figure 3, which decrease in the order Nb-(η^2-O_2), W-(η^2-O_2), and Ti-OOH. Lower LMCT energies correspond to more electrophilic reactive intermediates on groups 4−5 M-BEA. Active species on Ti-BEA absorb at lower energy wavelengths than those on Nb-BEA, which indicates a greater energy barrier to transfer charge to metal from the ligand, and therefore, the oxygen intermediates on Ti-BEA are more electrophilic than those on Nb-BEA. We reported previously that apparent activation enthalpies for cyclohexene epoxidation decrease linearly with the LMCT band for the reactive intermediate over groups 4−5 M-BEA.[13] Table 2 shows that the energies for LMCT from H_2O_2-derived species active for epoxidation on Ti-BEA and Nb-BEA lie at 3.1 eV (Ti-OOH) and 4.2 eV (Nb-(η^2-O_2)), respectively. In comparison, the LMCT energy for W-(η^2-O_2), the reactive species for W-BEA, falls between those for Nb-BEA and Ti-BEA at 3.6 eV, while Mo-BEA absorbs at energies similar to Ti-BEA. The values of these LMCT energies (Table 2) and the periodic trends for groups 4 and 5 metals led us to anticipate that epoxidation rates for W-BEA would fall between those for Ti-BEA and Nb-BEA (Ti-OOH > W-(η^2-O_2) > Nb-(η^2-O_2)) and that these differences would be reflected in apparent activation enthalpies for epoxidation. These expectations prove to be incorrect (*vide infra*).

3.2. *In Situ* Titrations of Active Sites. Equitable comparisons of turnover rates among M-BEA catalysts require accurate measurements for the density of catalytically active metal atoms within each material. Prior reports hypothesize that alkyl phosphonic acids deprotonate, and the conjugate bases bind strongly to Lewis acidic transition metal atoms grafted onto silica and inhibit catalytic turnovers.[12,48] The manner by which these titrants reduce reaction rates is not clear: phosphonic acids may inhibit the activation of H_2O_2 or make reactive M-OOH and M-(η^2-O_2) species inaccessible to the alkene. Figure 4 shows that epoxidation rates normalized by the total number of Ti atoms on Ti-BEA decrease as the ratio of methylphosphonic acid (MPA) or *tert*-butylphosphonic acid (TBPA) to Ti increases within the reaction mixtures. While 1-hexene epoxidation rates decrease modestly with the addition of MPA (e.g., ∼20% at equimolar quantities), cyclohexene epoxidation rates decrease linearly at lower ratios of MPA to Ti (Figure 4a) but retain a significant fraction of their initial value as the MPA-to-Ti ratio approaches unity. In comparison, TBPA inhibits epoxidation kinetics significantly for both 1-hexene and cyclohexene (Figure 4b). These comparisons suggest that neither MPA nor TBPA prevent the formation of H_2O_2-derived reactive intermediates. Rather, TBPA competitively binds to the active metal sterically inhibiting 1-hexene from accessing the reactive intermediate, Ti-OOH. This interpretation is supported by the differences between *in situ* UV−vis spectra of Ti-BEA with and without the addition of TBPA (Figure 4c). Contact with a H_2O_2 solution (10 mM H_2O_2, 39 mM H_2O, CH_3CN, 313 K) produces similar absorbance features on Ti-BEA samples in the presence and absence of TBPA, which demonstrates that significant coverages of Ti-(η^2-O_2) and Ti-OOH intermediates (section 3.1) form in both situations. The subsequent introduction of 1-hexene (0.1 M C_6H_{12}, 313 K, 60 min) leads to a significant decrease (30%) in the intensity of the LMCT feature in the absence of TBPA. However, contact with the same reactant solution causes a minimal attenuation of the absorbance feature (<10%) when TBPA binds to the Ti site. These observations indicate that phosphonic acid titrants inhibit epoxidation reactions because the bound complex sterically hinders the reaction between active M-(η^2-O_2) and M-OOH intermediates and alkene co-reagents but do not prevent the activation of H_2O_2.

Extrapolation of the initial linear regime of TBPA titration plots to the horizontal axis (Figure S8) provides estimates for the percentage of metal atoms that produce active sites in each M-BEA sample. These results of TBPA titrations indicate that nearly all Ti and Nb atoms within the BEA framework form active sites for 1-hexene epoxidation (Table 1); however, the portion of catalytically active W atoms is lower (70 ± 5%). The percentage of inactive W atoms increases with the mass loading of W on the dealuminated BEA zeolite (Figure S9), which correlates with a decrease in the band gap of these W-BEA samples from 4.41 to 4.10 eV (Table S2). Figure 5 shows that rates for 1-hexene epoxidation normalized by the total number of W atoms (determined by EDXRF) decrease monotonically as the W content increases. However, turnover rates determined by normalizing rates by the number of active

https://dx.doi.org/10.1021/acscatal.0c03394
ACS Catal. 2021, 11, 139−154

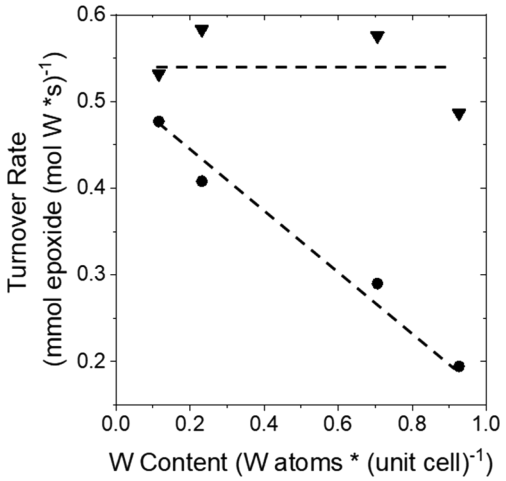

Figure 5. Rates for 1-hexene epoxidation in CH_3CN (10 mM C_6H_{12}, 1 mM H_2O_2, 3.9 mM H_2O, 313 K) normalized by the total number of W atoms (circle, solid ●) and by the number of active W atoms determined by TBPA site titrations (triangle, solid ▼) as functions of the tungsten content (W atoms (unit cell)$^{-1}$).

sites from TBPA titrations do not change across this range of W loadings (0.1−1 W atoms (unit cell)$^{-1}$), which suggests that oligomerization reduces the fraction of W atoms accessible to reactants. Consequently, we can accurately compare rates among M-BEA when we normalize to the amount of active metal measured by TBPA titrations. Moving forward, we report turnover rates by normalizing measured rates by the number of active sites within each M-BEA, as determined by TBPA titrations (Figure S8, Table 1).

3.3. Mechanistic Interpretation of Epoxidation Kinetics. Turnover rates for alkene epoxidation over Ti-BEA, Nb-BEA, and W-BEA depend on the concentration of the alkene, oxidant, and reaction products because the presence and concentration of these species determine the coverage of surface intermediates formed throughout the catalytic cycle. Scheme 2 depicts a catalytic cycle for epoxidation and H_2O_2 decomposition over group 4 metals, which can be extended to groups 5 and 6 and agrees with reported findings for cyclohexene,[13] 1-octene,[14] and styrene[3] epoxidation with H_2O_2 over Ti-, Nb-, and Ta-BEA catalysts and also with 1-octene epoxidation with *tert*-butyl hydroperoxide (TBHP) and cumene hydroperoxide (CHP) on Ti-BEA and Ti-SBA-15.[85] This series of elementary steps involves the quasi-equilibrated adsorption of C_6H_{12} (step 1) and H_2O_2 (step 2). Adsorbed H_2O_2 activates irreversibly (step 3) to form reactive M-OOH and M-(η^2-O_2). Subsequently, these intermediates transfer oxygen to C_6H_{12} in the kinetically relevant step for epoxidation (step 4) or decompose by reaction with fluid-phase H_2O_2 (step 6). Step 6, though depicted as a single elementary step, likely involves the homolysis of M-OOH or M-(η^2-O_2) moieties followed by rapid secondary reactions among radicals to form O_2 and H_2O, as proposed for Ti-silicates,[62] and regenerate the active site. Finally, $C_6H_{12}O$ desorbs in a quasi-equilibrated manner (step 5) to yield the epoxide product.

Figure 6 shows that turnover rates for 1-hexene (C_6H_{12}) epoxidation depend linearly on the concentration of C_6H_{12} ($[C_6H_{12}]$, where brackets denote the concentration of a species) and do not depend on $[H_2O_2]$ at low ratios of $[C_6H_{12}]$ to $[H_2O_2]$ on groups 4−6 M-BEA. At high ratios of $[C_6H_{12}]$ to $[H_2O_2]$, 1,2-epoxyhexane ($C_6H_{12}O$) formation rates increase in proportion to $[H_2O_2]$, depend weakly on $[C_6H_{12}]$, and depend inversely on $[C_6H_{12}O]$. These sets of coincident behavior signify two distinct kinetic regimes and agree with the mechanism depicted in Scheme 2. Both involve kinetically relevant O-atom transfer from H_2O_2-derived

Scheme 2. Proposed Mechanism for 1-Hexene Epoxidation with H_2O_2 and H_2O_2 Decomposition Depicted for Group 4 M-BEA. The ⇌ Symbol Denotes a Quasi-Equilibrated Step, and the ↛ Symbol Signifies the Kinetically Relevant Steps for the Formation of Distinct Products. Solvent Molecules Have Been Omitted for Clarity

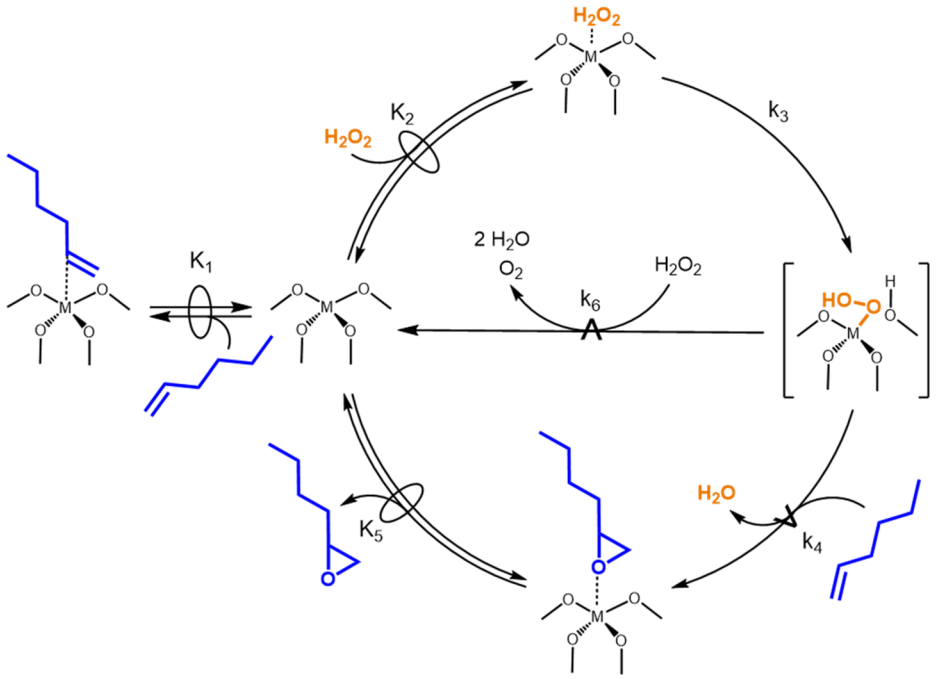

https://dx.doi.org/10.1021/acscatal.0c03394
ACS Catal. 2021, 11, 139−154

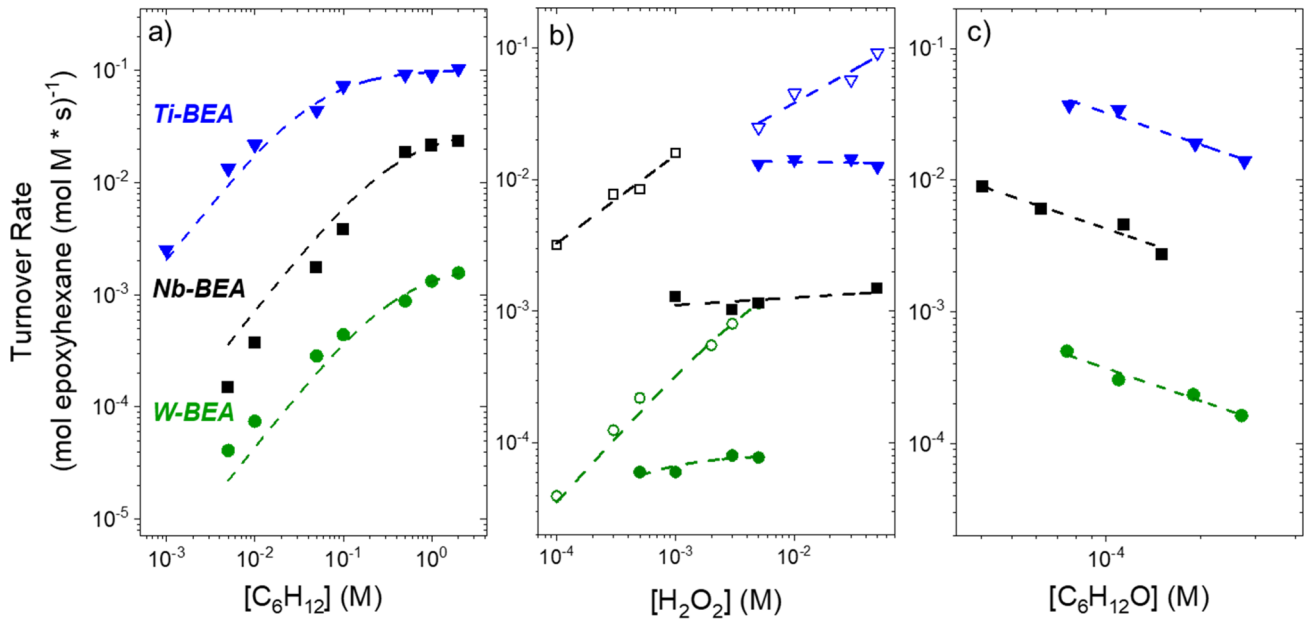

Figure 6. Turnover rates for 1,2-epoxyhexane formation in CH_3CN as a function of (a) $[C_6H_{12}]$ over Ti-BEA (blue triangle, solid ▼, 10 mM H_2O_2), Nb-BEA (black square, solid ■, 1 mM H_2O_2), and W-BEA (green circle, solid ●, 1 mM H_2O_2); (b) $[H_2O_2]$ over Ti-BEA (blue triangle, solid ▼, 0.1 mM C_6H_{12}; blue triangle, open ▽, 1 M C_6H_{12}), Nb-BEA (black square, solid ■, 0.5 mM C_6H_{12}; black square, open □, 2 M C_6H_{12}), and W-BEA (green circle, solid ●, 0.5 mM C_6H_{12}; green circle, open ○, 2 M C_6H_{12}); (c) $[C_6H_{12}O]$ over Ti-BEA (blue triangle, solid ▼, 2 M C_6H_{12}, 10 mM H_2O_2), Nb-BEA (black square, solid ■, 1 M C_6H_{12}, 1 mM H_2O_2), and W-BEA (green circle, solid ●, 2 M C_6H_{12}, 1 mM H_2O_2).

reactive intermediates to C_6H_{12} (see section 3.1); however, the prevailing surface intermediates differ. The first regime contains activated forms of H_2O_2 as the most abundant reactive intermediates (MARI), and the second regime presents sites predominantly covered by the epoxide product. Scheme 2 indicates that rates for epoxidation (r_E) shown in Figure 6 can be predicted by a rate expression with the form

$$r_E = k_4[M - OOH][C_6H_{12}] \quad (1)$$

where k_4 is the rate constant for step 4 in Scheme 2, and [M − OOH] represents the number of H_2O_2-activated metal sites (the sum of both M-OOH and M-(η^2-O_2)). The functional dependence of r_E on reactant concentrations becomes apparent following the use of the pseudo-steady-state hypothesis to determine [M − OOH] and by requiring that the sum of all adsorbed species equals the total number of active sites ([L]).[3,13,14,86] This treatment yields

$$\frac{r_E}{[L]} = \frac{\frac{k_3k_4K_2[H_2O_2][C_6H_{12}]}{k_4[C_6H_{12}] + k_6[H_2O_2]}}{1 + K_1[C_6H_{12}] + K_2[H_2O_2] + \frac{k_3K_2[H_2O_2]}{k_4[C_6H_{12}] + k_6[H_2O_2]} + \frac{[C_6H_{12}O]}{K_5}} \quad (2)$$

where the five terms in the denominator represent the numbers of sites occupied by the solvent CH_3CN, C_6H_{12}, H_2O_2, activated forms of H_2O_2, and 1,2-epoxyhexane, respectively. The full derivation of eq 2 is shown in the Supporting Information (section S5.0).

At low alkene concentrations, the activated form of H_2O_2 becomes the MARI, and consequently, the rate expression (eq 2) simplifies to

$$\frac{r_E}{[L]} = k_4[C_6H_{12}] \quad (3)$$

which predicts rates that match the observed near-first-order dependence on $[C_6H_{12}]$ and the lack of dependence on $[H_2O_2]$. High ratios of $[C_6H_{12}]$ to $[H_2O_2]$ cause $C_6H_{12}O$ to saturate active sites, and the rate expression becomes

$$\frac{r_E}{[L]} = \frac{k_3k_4K_2K_5[H_2O_2][C_6H_{12}]}{[C_6H_{12}O](k_4[C_6H_{12}] + k_6[H_2O_2])} \quad (4)$$

Eq 4 applies to all groups 4−6 M-BEA and describes trends in Figure 6 near greater $[C_6H_{12}]$ and lower $[H_2O_2]$ values. This rate expression simplifies further for catalysts with high selectivities for epoxidation (e.g., Ti-BEA selectivities >90%, section 3.4) because the rate of epoxidation far exceeds that of H_2O_2 decomposition ($k_4[C_6H_{12}] >> k_6[H_2O_2]$) such that:

$$\frac{r_E}{[L]} = \frac{k_3K_2K_5[H_2O_2]}{[C_6H_{12}O]} \quad (5)$$

which agrees with the experimentally observed kinetic regime for Ti-BEA at a high $[C_6H_{12}]$-to-$[H_2O_2]$ ratio where turnover rates do not depend on $[C_6H_{12}]$. Here, the MARI shifts from H_2O_2-derived species to a C_6H_{12}-derived MARI indicated by a near-first-order dependence on H_2O_2 and a negative dependence on $C_6H_{12}O$ at high ratios of $[C_6H_{12}]$ to $[H_2O_2]$. The rate expression and corresponding derivation for decomposition of H_2O_2 (step 6) are given in the Supporting Information (section S5.0).

Rate measurements for 1-hexene epoxidation with H_2O_2 over Ti-, Nb-, and W-BEA suggest that all these catalysts utilize the same elementary steps and similar transition states to achieve epoxidations (Scheme 2). Yet, epoxidation turnover rates on Ti-BEA are 250- and 60-fold greater than W-BEA and Nb-BEA, respectively, at comparable conditions. These large differences in turnover rates reflect variations in electron affinities of the active sites and stability of the adsorbed epoxide as described next.

https://dx.doi.org/10.1021/acscatal.0c03394
ACS Catal. 2021, 11, 139−154

Scheme 3. Changes in Enthalpy that Correspond to (a) the Formation of the Transition State for Epoxidation ($\Delta H^{\ddagger}_{epox}$) and the Epoxide ($\Delta H_{rxn}$) from C_6H_{12} and a M-OOH Intermediate and (b) the Adsorption of 1,2-Epoxyhexane to the Active Site of an M-BEA Catalyst (Depicted for a Group 4 Metal)

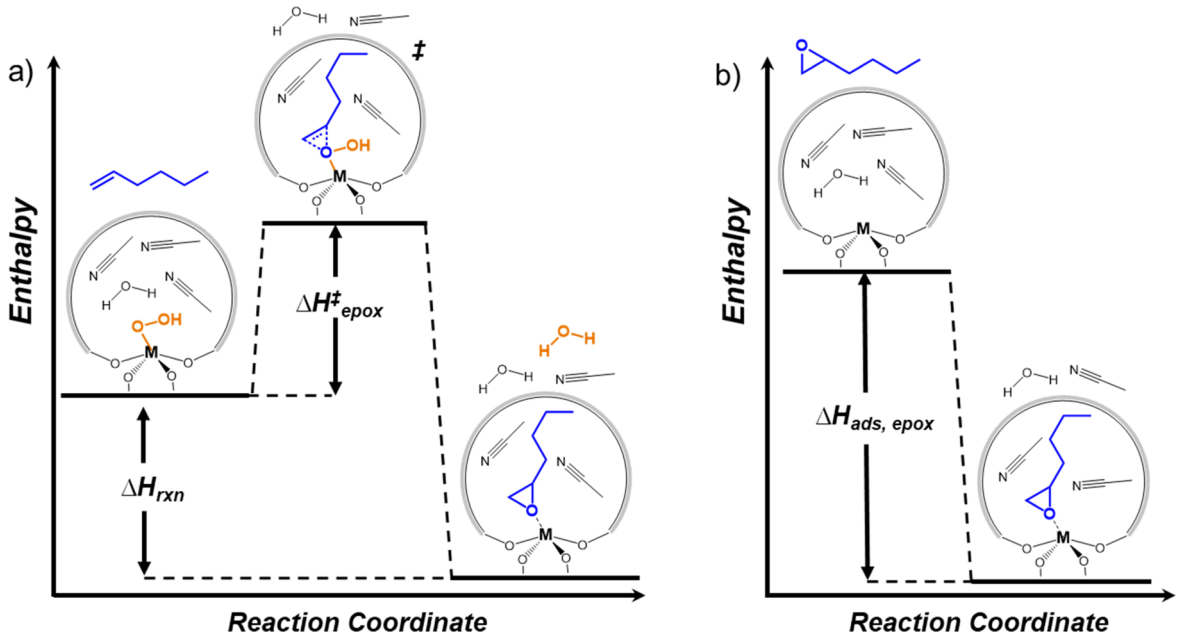

3.4. Linear Free-Energy Relationships for Alkene Epoxidation and H_2O_2 Decomposition. Activation enthalpies (and free energies) for elementary steps depend intimately upon the reaction enthalpies (and free energies) of the same step, as postulated by Hammond.[87,88] Recently, we demonstrated that heats of adsorption of pyridine (C_5H_5N) and deuterated acetonitrile (CD_3CN) in the gas-phase linearly correlate to activation enthalpies for liquid-phase epoxidation and H_2O_2 decomposition on groups 4−5 transition-metal-bearing zeolite BEA.[3,11,14] These linear relationships suggest that groups 4−5 M-BEA that bind basic molecules with increasing stability, quantified as a functional measure of Lewis acid strength, have lower activation enthalpies for liquid-phase epoxidation. While these measurements imply the intrinsic electronic interactions between the transition state and active site, they do not capture other forms of chemical interactions that affect the rate and equilibrium constants pertinent for this reaction. Scheme 3 illustrates that the formation of the transition state that forms 1,2-epoxyhexane within the pores of M-BEA requires the displacement and reorganization of solvent molecules (Scheme 3a) in ways that should closely resemble the structural changes induced by adsorption of the epoxide product (Scheme 3b). Excess free-energy contributions that originate from interactions between the transition state, geminal chemical bound to the active site (e.g., hydroxyl or oxos on W atoms), solvent, and extended surface of the pores will affect both processes, as demonstrated by linear free-energy relationships (LFER) for 1-octene epoxidation across a range of Ti-BEA catalysts with different densities of silanol groups (i.e., hydrophilicities).[11] Here, we account for these additional interactions within linear free-energy relationships by using isothermal titration calorimetry (ITC) to directly measure the adsorption enthalpy of 1,2-epoxyhexane ($\Delta H_{ads,epox}$) onto M-BEA in the aqueous acetonitrile reaction solvent. 1,2-Epoxyhexane is a suitable titrant for these measurements (e.g., rather than pyridine, an alkene, or an epoxide with a different alkyl group) because measured heats of adsorption reflect a combination of specific and nonspecific interactions between the adsorbate, framework metal atom, zeolite pore wall, and confined solvent molecules. Specifically, we expect a certain enthalpic stabilization from the interaction between the oxirane ring and framework metal center but also contributions from solvent displacement and restructuring that reflect the size of the epoxide (i.e., the van der Waals volume and surface area). Consequently, we anticipated that 1,2-epoxyhexane and values for $\Delta H_{ads,epox}$ would serve as the most representative surrogate for the epoxide-like transition state (Scheme 3) and the complete set of interactions with its surroundings.

Figure 7 presents apparent activation enthalpies for 1-hexene epoxidation ($\Delta H^{\ddagger}_{epox}$, Scheme 3a) and H_2O_2 decomposition

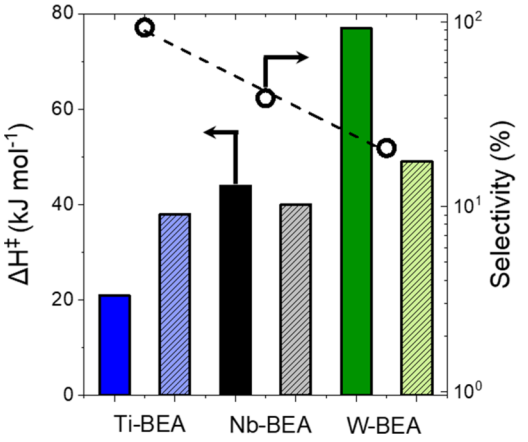

Figure 7. Apparent activation enthalpies ($\Delta H^{\ddagger}_{epox}$, solid bars; $\Delta H^{\ddagger}_{dec}$, dashed bars) and 1-hexene epoxidation selectivities on M-OOH saturated sites in CH_3CN (303−333 K) for Ti-BEA (0.5 mM C_6H_{12}, 10 mM H_2O_2, 39 mM H_2O), Nb-BEA (5 mM C_6H_{12}, 1 mM H_2O_2, 3.9 mM H_2O), and W-BEA (5 mM C_6H_{12}, 1 mM H_2O_2, 3.9 mM H_2O).

https://dx.doi.org/10.1021/acscatal.0c03394
ACS Catal. 2021, 11, 139−154

($\Delta H^{\ddagger}_{dec}$) measured on M-OOH saturated sites for all M-BEA to enable equitable comparisons between materials. The differences in $\Delta H^{\ddagger}_{epox}$ (21−77 kJ mol^{-1}) and $\Delta H^{\ddagger}_{dec}$ (38−49 kJ mol^{-1}) between group 4−6 M-BEA for 1-hexene epoxidation are consistent with previous reports for cyclohexene[13] and styrene[3] epoxidation with H_2O_2, where lower $\Delta H^{\ddagger}_{epox}$ corresponds to higher rates and selectivities for epoxidation over M-BEA (Figure 7).

Values of $\Delta H_{ads,epox}$ were measured by ITC in liquid solutions with compositions that resemble the reaction solvent. We titrated a slurry of ∼20−30 mg of M-BEA in CH_3CN (39 mM H_2O, 313 K) with a solution of 1,2-epoxyhexane in CH_3CN (39 mM H_2O, 313 K). Figure 8 depicts a

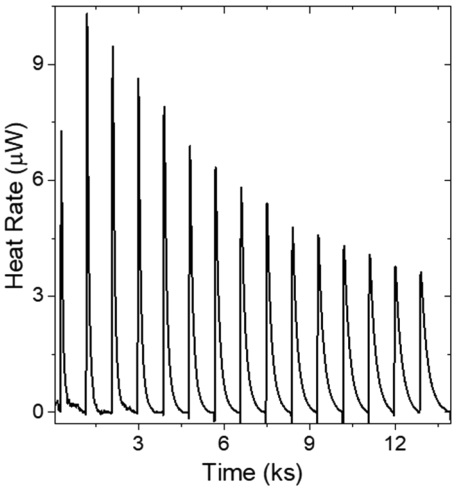

Figure 8. Thermogram from the titration of W-BEA with 1,2-epoxyhexane (10 mM $C_6H_{12}O$ in CH_3CN) during isothermal titration calorimetry (39 mM H_2O, 313 K, 1 uL per injection).

representative thermogram for 1 μL injections of the titrant solution in which the titrant coverage increases with the number of injections and time. As the experiment proceeds, the areas for peaks remain nearly constant but the maximum intensity decreases because 1,2-epoxyhexane must diffuse further into the M-BEA particles to access unoccupied sites. Figure 9 shows heats measured for each injection, which represent the peak areas in Figure 8 normalized by the number of 1,2-epoxyhexane molecules within each injection. These measurements were performed at low titrant-to-metal atom ratios ($\theta_{epox,M}$ <0.2) to ensure every titrant molecule binds to active sites (all isotherms and thermograms are displayed in Figure S10). Table 3 contains the measured enthalpies of adsorption for 1,2-epoxyhexane ($\Delta H_{ads,epox}$) for Ti-BEA, Nb-BEA, and W-BEA, and these values show that $C_6H_{12}O$ binds most strongly to Ti active sites (−134 ± 2 kJ mol^{-1}) and least strongly to W active sites (−97 ± 2 kJ mol^{-1}). Comparisons of heats of adsorption for $C_6H_{12}O$, CD_3CN,[3,13] (Table 3), and C_5H_5N indicate that basic molecules consistently bind more exothermically to framework Ti sites than to Nb sites and support the idea that Ti atoms have greater electron affinities than Nb or W atoms in the BEA framework.

The observed trends for both apparent activation enthalpies ($\Delta H^{\ddagger}_{epox}$, $\Delta H^{\ddagger}_{dec}$; Figure 7) and adsorption enthalpies (e.g., $\Delta H_{ads,epox}$; Table 3) demonstrate that W-BEA stabilizes transition states and products for epoxidation less effectively than Ti-BEA and Nb-BEA, despite the greater electronegativity of W.

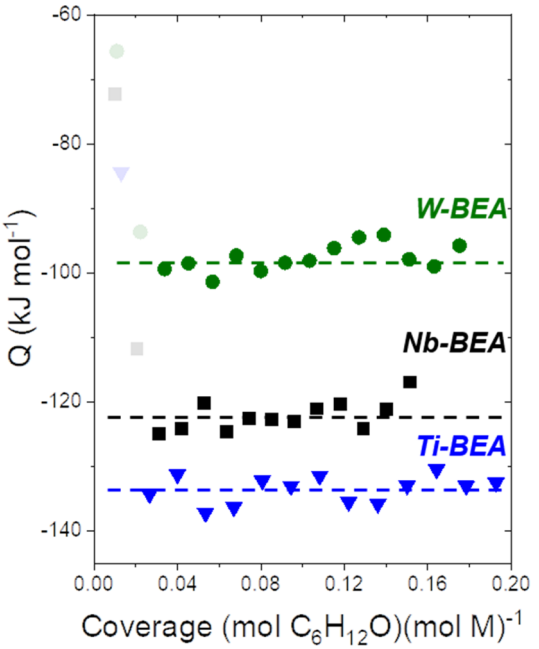

Figure 9. Heats released upon 1,2-epoxyhexane adsorption in CH_3CN (39 mM H_2O, 313 K) on Ti-BEA (blue triangle ▼), Nb-BEA (black square ■), and W-BEA (green circle ●) as a function of 1,2-epoxyhexane coverage. Transparent points are omitted from analysis due to common errors associated with early injections.

Table 3. Adsorption Enthalpies for 1,2-Epoxyhexane and CD_3CN on M-BEA

catalyst	$\Delta H_{ads,epox}$[a] (kJ mol^{-1})	$\Delta H_{ads,CD3CN}$[b] (kJ mol^{-1})
Ti-BEA	−134 ± 2	−31 ± 2
Nb-BEA	−122 ± 2	−22 ± 2
W-BEA	−97 ± 2	n.d.[c]

[a]Titrant surface coverage is 0−0.2 mol 1,2-epoxyhexane (mol metal)$^{-1}$ (39 mM H_2O in CH_3CN, 313 K, 250 rpm). [b]Values taken from Reference 3. [c]Not determined because CD_3CN deactivates Lewis acid sites on W-BEA at temperatures >373 K.

We hypothesized that W, the most electronegative among the metals incorporated into BEA (Figure S11), would present the smallest $\Delta H^{\ddagger}_{epox}$ by withdrawing electron density from reactive oxygen species and increasing their electrophilicity. The Pauling and Sanderson electronegativities of these elements do not correlate to either $\Delta H^{\ddagger}_{epox}$ or $\Delta H_{ads,epox}$ values on these M-BEA. These electronegativity scales reflect elemental properties that apparently do not extend accurately to groups 4−6 metals as present in the zeolite framework. The lack of correlation is not surprising because these metals acquire distinct coordination structures to framework of BEA and different numbers and types of geminal oxygen functions.

Mulliken electronegativities correlate linearly with values of $\Delta H^{\ddagger}_{epox}$, $\Delta H^{\ddagger}_{dec}$, and $\Delta H_{ads,epox}$; however, these relationships contradict our initial hypothesis and indicate that the metals with greater electron affinities give rise to weaker adsorption of 1,2-epoxyhexane (Figure S11a) and greater $\Delta H^{\ddagger}_{epox}$ (Figure S11b). Mulliken electronegativities represent an average of the electron affinity and the first ionization energy of a given element,[89] but these calculations cannot account for differences in oxidation states, the number and types of ligands, or bond angles and lengths for the metal as it exists during catalysis in BEA. These realizations and the nonintuitive

https://dx.doi.org/10.1021/acscatal.0c03394
ACS Catal. 2021, 11, 139−154

anticorrelation between $\Delta H_{ads,epox}$ and Mulliken electronegativites show the need to interrogate molecular interactions at these sites experimentally.

Despite these complicating factors, Figure 10 shows that values of $\Delta H^{\ddagger}_{epox}$ and $\Delta H^{\ddagger}_{dec}$ decrease linearly as $\Delta H_{ads,epox}$

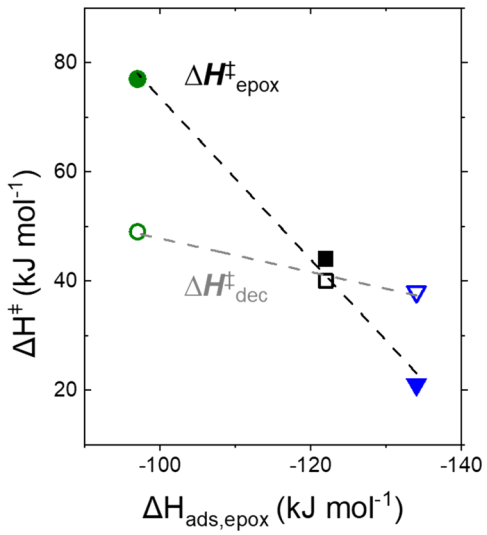

Figure 10. Apparent activation barriers for 1-hexene epoxidation in CH_3CN over Ti-BEA (blue triangle, solid ▼, 0.5 mM C_6H_{12}, 10 mM H_2O_2), Nb-BEA (black square, solid ■, 5 mM C_6H_{12}, 1 mM H_2O_2), and W-BEA (green circle, solid ●, 5 mM C_6H_{12}, 1 mM H_2O_2); and H_2O_2 decomposition in CH_3CN over Ti-BEA (blue triangle, open ▽, 1 mM H_2O_2, 3.9 mM H_2O), Nb-BEA (black square, open □, 1 mM H_2O_2, 3.9 mM H_2O), and W-BEA (green circle, open ○, 1 mM H_2O_2, 3.9 mM H_2O) as functions of 1,2-epoxyhexane heat of adsorption on M-BEA (W, green circle, solid ●, green circle, open ○; Nb, black square, solid ■, black square, open □; Ti, blue triangle, solid ▼, blue triangle, open ▽).

values increase for Ti-, Nb, and W-BEA. The linear free-energy relationship for $\Delta H^{\ddagger}_{epox}$ demonstrates that the interactions of 1,2-epoxyhexane with active sites (and their distinct sets of hydroxyl and oxo groups) resemble closely the interactions of the transition state for epoxidation and obeys Hammond's postulate notwithstanding the significant differences between the structure of active sites. Notably, $\Delta H^{\ddagger}_{epox}$ is more sensitive to $\Delta H_{ads,epox}$ (slope of correlation equal to 1.5 ± 0.2, Figure 10), which must stem from the structural similarities between the transition state and adsorbate. These similarities cause the adsorbate to experience a combination of covalent, specific (e.g., hydrogen-bonding with the solvent and pore wall) and non-specific (van der Waals forces) interactions comparable to those that act upon the transition state. Values for $\Delta H^{\ddagger}_{dec}$ also scale linearly with $\Delta H_{ads,epox}$ but do so much more weakly (slope equal to 0.30 ± 0.01, Figure 10) because both the covalent and (non)specific interactions differ between the transition state for H_2O_2 decomposition and adsorbed 1,2-epoxyhexane, as expected. These trends in $\Delta H_{ads,epox}$ values show that the lone pairs of the oxirane ring bind more strongly to Ti- and Nb-atoms in BEA, which implies that these sites have greater electron affinities than W-atoms. The electron affinity of these sites impacts catalysis by regulating the electrophilicity of reactive oxygen species that exchange electrons with the electron-rich C═C bonds of C_6H_{12} and attack H_2O_2.

Notably, these trends in turnover rates and activation barriers differ from those previously reported for Ti and Nb silicates[4,17,24] and Ti and Nb-POMs[21,22] where Nb materials revealed lower activation barriers and higher rates and selectivities for cyclooctene and cyclohexene epoxidation than those measured for their Ti counterparts. These differences could be attributed to several factors, which include the relevance of distinct reactive intermediates between these studies and differences between the structure and form of the support for the active sites (e.g., tungstate POM or BEA zeolite). Here, we compared turnover rates and measured $\Delta H^{\ddagger}_{epox}$ at reaction conditions that ensured that H_2O_2-derived intermediates comprised the MARI upon all M-BEA catalysts. The reaction conditions employed to obtain activation energy measurements in prior work appear to result in active sites that are covered by several surface intermediates (i.e., both those derived from H_2O_2 and cyclooctene) that exist at comparable coverages.[24] In addition, the supports that bind the active Ti and Nb differ significantly (i.e., amorphous silicates, Lindqvist-type tungstate POM, and BEA zeolite). Despite differences between the relative epoxidation turnover rates and apparent activation barriers among Ti-, Nb-, and W-BEA catalysts and those in prior reports on Ti- and Nb-silicate and POM materials, the findings among all reports do agree with the broad conclusion that active sites with greater electrophilicity (or Lewis acidity) provide higher turnover rates and lower activation barriers. We have directly examined the electrophilicity of sites in M-BEA catalysts by comparisons between LMCT energies obtained by *in situ* UV−vis experiments and quantified the enthalpy of adsorption of 1,2-epoxyhexane (a transition state mimic) by isothermal titration calorimetry. Both methods demonstrate that Ti-BEA presents active sites with greater electrophilicities (and greater Lewis acid strength) than Nb-BEA, which agrees with the considerably lower activation enthalpies for epoxidations on Ti-BEA and current understanding of structure function relationships for epoxidation catalysts.

4. CONCLUSIONS

Differences in the elemental identity of metal atoms substituted into the framework of zeolite catalysts influence rates and selectivities for alkene epoxidation reactions, and other liquid-phase chemistries, by stabilizing reactive intermediates and transition states through combinations of covalent, specific, and nonspecific interactions. These differences cannot be accurately predicted based upon intrinsic properties (e.g., electronegativities) of the transition-metal elements that form active sites alone; however, Hammond's postulate provides guidance for developing simple methods to probe the combination of these interactions using adsorption measurements. These concepts were investigated here by examining H_2O_2 activation and 1-hexene epoxidation over a series of groups 4−6 transition-metal-substituted zeolite BEA catalysts, which possess predominantly monomeric metal atoms located at tetrahedral positions of the BEA framework. *In situ* UV−vis and Raman spectroscopy show that these M-BEA materials form similar pools of reactive oxygen intermediates (M-OOH and M-(η^2-O_2)) following H_2O_2 activation; however, products of *cis*-stilbene epoxidation indicate that M-OOH intermediates dominate epoxidations on Ti-BEA while M-(η^2-O_2) are responsible for reactions on Nb- and W-BEA. 1-Hexene epoxidation occurs within Ti-, Nb-, and W-BEA catalysts with functionally identical dependencies

https://dx.doi.org/10.1021/acscatal.0c03394
ACS Catal. 2021, 11, 139−154

on C_6H_{12} and H_2O_2 concentrations, despite differences in rates that span two-orders of magnitude. Comparisons across these M-BEA catalysts at comparable conditions show epoxidation selectivities are the greatest on Ti-BEA (93%), followed by Nb- (38%) and W-BEA (20%) and turnover rates (determined using *in situ* site titrations) are 250- and 60-fold lower on W-BEA and Nb-BEA than Ti-BEA, respectively. These large kinetic differences result from differences in the stability of the epoxidation transition state, relative to the reactive M-OOH intermediates, and not from differences in mechanism or numbers of active sites.

The stability of transition states is inferred through measurements of apparent activation enthalpies ($\Delta H^{\ddagger}$) and do not correlate with measures of the electronegativities of the transition-metal atoms located within the framework of zeolite BEA. The lack of correlation suggests that these active sites stabilize transition states through a collection of interactions that cannot be completely described by the tendency of the metal atom to attract electrons and must be assessed by a more comprehensive probe of the interactions. Liquid-phase adsorption enthalpies of 1,2-epoxyhexane ($\Delta H_{ads,epox}$) measured within the reaction solvent by isothermal titration calorimetry (ITC) provides one method for quantifying the complete set of interactions. Values of $\Delta H_{ads,epox}$ show W-BEA binds 1,2-epoxyhexane less strongly than Ti- and Nb-BEA, even though W was anticipated to possess the greatest electron affinity, which suggests that differences between the structure and coordination of these metal atoms within the BEA framework introduce catalytically consequential variations in the electronic structure of the metal site and the number and nature of pendant functional groups (e.g., −OH, =O, SiOH) that interact directly and indirectly with transition states. $\Delta H^{\ddagger}$ values for epoxidation and H_2O_2 decomposition decrease linearly as the adsorption of the epoxide becomes more exothermic, which shows that 1-hexene epoxidation follows a simple linear free-energy relationship that provides a more meaningful descriptor for catalytic performance than tabulated electronegativities of the elements within these zeolite catalysts.

The relationships developed between these kinetic, spectroscopic, and calorimetric studies provide an explanation for the differences in the observed epoxidation turnover rates, selectivity, and apparent activation enthalpies for M-BEA catalysts. These findings suggest rates and selectivities for epoxidation reactions can be improved simultaneously by increasing the functional electron affinity (or Lewis acidity) of active sites within zeolite frameworks and that reported electronegativities of elements do not provide a sufficient description to predict the behavior of the active sites in various coordination environments. Moreover, these results serve to remind us of the insights gained from constructing appropriate comparisons between kinetic and thermodynamic properties of catalytic materials in complex environments.

■ ASSOCIATED CONTENT

Supporting Information

The Supporting Information is available free of charge at https://pubs.acs.org/doi/10.1021/acscatal.0c03394.

Diffuse-reflectance UV−vis, X-ray diffraction, *ex situ* Raman spectroscopy, *in situ* UV−vis and Raman spectroscopy, *cis*-stilbene epoxidation kinetics, *in situ* phenyl phosphonic acid site titrations, and activation enthalpies and heats of adsorption as functions of active metal electronegativity (PDF)

■ AUTHOR INFORMATION

Corresponding Author

David W. Flaherty − *Department of Chemical and Biomolecular Engineering, University of Illinois at Urbana-Champaign, Urbana, Illinois 61801, United States;* orcid.org/0000-0002-0567-8481; Email: dwflhrty@illinois.edu

Authors

E. Zeynep Ayla − *Department of Chemical and Biomolecular Engineering, University of Illinois at Urbana-Champaign, Urbana, Illinois 61801, United States*

David S. Potts − *Department of Chemical and Biomolecular Engineering, University of Illinois at Urbana-Champaign, Urbana, Illinois 61801, United States;* orcid.org/0000-0001-8303-7359

Daniel T. Bregante − *Department of Chemical and Biomolecular Engineering, University of Illinois at Urbana-Champaign, Urbana, Illinois 61801, United States;* orcid.org/0000-0003-2157-1286

Complete contact information is available at: https://pubs.acs.org/10.1021/acscatal.0c03394

Author Contributions

All authors have given approval to the final version of the manuscript.

Notes

The authors declare no competing financial interest.

■ ACKNOWLEDGMENTS

We thank Professor Damien Guironnet for use of laboratory equipment for the synthesis of M-BEA and Arzam Harris for technical assistance. EDXRF, XRD, and DRUVS were carried out in the Frederick Seitz Materials Research Laboratory at the University of Illinois. This work was supported by the U.S. Army Research Office under grant number W911NF-18-1-0100. D.T.B. and D.S.P. were supported by the U.S. Department of Energy (DE-SC0020224). EZA acknowledges the SURGE Fellowship through the University of Illinois.

■ REFERENCES

(1) Oyama, S. T. *Mechanisms in Homogeneous and Heterogeneous Epoxidation Catalysis*; Elsevier: 2008; p 528.

(2) Bregante, D. T.; Tan, J. Z.; Sutrisno, A.; Flaherty, D. W. Heteroatom substituted zeolite FAU with ultralow Al contents for liquid-phase oxidation catalysis. *Catal. Sci. Technol.* **2020**, *10*, 635−647.

(3) Bregante, D. T.; Thornburg, N. E.; Notestein, J. M.; Flaherty, D. W. Consequences of Confinement for Alkene Epoxidation with Hydrogen Peroxide on Highly Dispersed Group 4 and 5 Metal Oxide Catalysts. *ACS Catal.* **2018**, *8*, 2995−3010.

(4) Thornburg, N. E.; Thompson, A. B.; Notestein, J. M. Periodic Trends in Highly Dispersed Groups IV and V Supported Metal Oxide Catalysts for Alkene Epoxidation with H_2O_2. *ACS Catal.* **2015**, *5*, 5077−5088.

(5) Corma, A.; Navarro, M. T.; Pariente, J. P. R. Synthesis of an ultralarge pore titanium silicate isomorphous to MCM-41 and its application as a catalyst for selective oxidation of hydrocarbons. *J. Chem. Soc., Chem. Commun.* **1994**, 147.

(6) Aigner, M.; Grosso-Giordano, N. A.; Okrut, A.; Zones, S.; Katz, A. Epoxidation of 1-octene under harsh tail-end conditions in a flow

reactor I: a comparative study of crystalline *vs*.amorphous catalysts. *React. Chem. Eng.* **2017**, *2*, 842−851.
(7) Wu, P.; Tatsumi, T.; Komatsu, T.; Yashima, T. A Novel Titanosilicate with MWW Structure: II. Catalytic Properties in the Selective Oxidation of Alkenes. *J. Catal.* **2001**, *202*, 245−255.
(8) Riedel, D. H. T. J.; Wegerle, U.; Parvulescu, A.-N.; Schroeder, A.; Spiske, L.; Urbanczyk, D.; Mueller, U.; Witzl, W.; Weidenbach, M. Process for preparing propylene oxide. U.S. Patent 9,738,616 B2, 2017.
(9) Nijhuis, T. A.; Makkee, M.; Moulijn, J. A.; Weckhuysen, B. M. The Production of Propene Oxide: Catalytic Processes and Recent Developments. *Ind. Eng. Chem. Res.* **2006**, *45*, 3447−3459.
(10) Nijhuis, T. A.; Huizinga, B. J.; Makkee, M.; Moulijn, J. A. Direct Epoxidation of Propene Using Gold Dispersed on TS-1 and Other Titanium-Containing Supports. *Ind. Eng. Chem. Fundam.* **1999**, *38*, 884−891.
(11) Bregante, D. T.; Flaherty, D. W. Impact of Specific Interactions Among Reactive Surface Intermediates and Confined Water on Epoxidation Catalysis and Adsorption in Lewis Acid Zeolites. *ACS Catal.* **2019**, 10951−10962.
(12) Thornburg, N. E.; Nauert, S. L.; Thompson, A. B.; Notestein, J. M. Synthesis−Structure−Function Relationships of Silica-Supported Niobium(V) Catalysts for Alkene Epoxidation with H_2O_2. *ACS Catal.* **2016**, *6*, 6124−6134.
(13) Bregante, D. T.; Flaherty, D. W. Periodic Trends in Olefin Epoxidation over Group IV and V Framework-Substituted Zeolite Catalysts: A Kinetic and Spectroscopic Study. *J. Am. Chem. Soc.* **2017**, *139*, 6888−6898.
(14) Bregante, D. T.; Johnson, A. M.; Patel, A. Y.; Ayla, E. Z.; Cordon, M. J.; Bukowski, B. C.; Greeley, J.; Gounder, R.; Flaherty, D. W. Cooperative Effects between Hydrophilic Pores and Solvents: Catalytic Consequences of Hydrogen Bonding on Alkene Epoxidation in Zeolites. *J. Am. Chem. Soc.* **2019**, *141*, 7302−7319.
(15) Joergensen, K. A. Transition-metal-catalyzed epoxidations. *Chem. Rev.* **1989**, *89*, 431−458.
(16) Notestein, J. M.; Iglesia, E.; Katz, A. Grafted Metallocalixarenes as Single-Site Surface Organometallic Catalysts. *J. Am. Chem. Soc.* **2004**, *126*, 16478−16486.
(17) Ivanchikova, I. D.; Skobelev, I. Y.; Maksimchuk, N. V.; Paukshtis, E. A.; Shashkov, M. V.; Kholdeeva, O. A. Toward understanding the unusual reactivity of mesoporous niobium silicates in epoxidation of C C bonds with hydrogen peroxide. *J. Catal.* **2017**, *356*, 85−99.
(18) Corma, A.; Fornes, V.; Pergher, S. B.; Maesen, T. L. M.; Buglass, J. G. Delaminated zeolite precursors as selective acidic catalysts. *Nature* **1998**, *396*, 353−356.
(19) Antonova, N. S.; Carbó, J. J.; Kortz, U.; Kholdeeva, O. A.; Poblet, J. M. Mechanistic Insights into Alkene Epoxidation with H_2O_2 by Ti- and other TM-Containing Polyoxometalates: Role of the Metal Nature and Coordination Environment. *J. Am. Chem. Soc.* **2010**, *132*, 7488−7497.
(20) Jiménez-Lozano, P.; Skobelev, I. Y.; Kholdeeva, O. A.; Poblet, J. M.; Carbó, J. J. Alkene Epoxidation Catalyzed by Ti-Containing Polyoxometalates: Unprecedented β-Oxygen Transfer Mechanism. *Inorg. Chem.* **2016**, *55*, 6080−6084.
(21) Maksimchuk, N. V.; Ivanchikova, I. D.; Maksimov, G. M.; Eltsov, I. V.; Evtushok, V. Y.; Kholdeeva, O. A.; Lebbie, D.; Errington, R. J.; Solé-Daura, A.; Poblet, J. M.; Carbó, J. J. Why Does Nb(V) Show Higher Heterolytic Pathway Selectivity Than Ti(IV) in Epoxidation with H_2O_2? Answers from Model Studies on Nb- and Ti-Substituted Lindqvist Tungstates. *ACS Catal.* **2019**, 6262−6275.
(22) Maksimchuk, N. V.; Maksimov, G. M.; Evtushok, V. Y.; Ivanchikova, I. D.; Chesalov, Y. A.; Maksimovskaya, R. I.; Kholdeeva, O. A.; Solé-Daura, A.; Poblet, J. M.; Carbó, J. J. Relevance of Protons in Heterolytic Activation of H2O2over Nb(V): Insights from Model Studies on Nb-Substituted Polyoxometalates. *ACS Catal.* **2018**, *8*, 9722−9737.
(23) Boronat, M.; Corma, A.; Renz, M.; Viruela, P. M. Predicting the Activity of Single Isolated Lewis Acid Sites in Solid Catalysts. *Chem. − Eur. J.* **2006**, *12*, 7067−7077.
(24) Kholdeeva, O. A.; Ivanchikova, I. D.; Maksimchuk, N. V.; Skobelev, I. Y. H2O2-based selective epoxidations: Nb-silicates versus Ti-silicates. *Catal. Today* **2019**, *333*, 63−70.
(25) Oxtoby, D. W.; Gillsi, H. P.; Campion, A. *Principles of Modern Chemistry*. 7th ed.; Cengage Learning: 2012.
(26) Sheldon, R. A. Synthetic and mechanistic aspects of metal-catalysed epoxidations with hydroperoxides. *J. Mol. Catal.* **1980**, *7*, 107−126.
(27) Sheldon, R. Metal-catalyzed epoxidation of olefins with organic hydroperoxides I. A comparison of various metal catalysts. *J. Catal.* **1973**, *31*, 427−437.
(28) Mimoun, H. Do metal peroxides as homolytic and heterolytic oxidative reagents. Mechanism of the halcon epoxidation process. *Catal. Today* **1987**, *1*, 281−295.
(29) Buijink, J. K. F.; Van Vlaanderen, J. J. M.; Crocker, M.; Niele, F. G. M. Propylene epoxidation over titanium-on-silica catalyst—the heart of the SMPO process. *Catal. Today* **2004**, *93-95*, 199−204.
(30) Chiusoli, G. P., Maitlis, P. M., *Metal-catalysis in Industrial Organic Processes*. Royal Society of Chemistry: 2006.
(31) Amini, M.; Haghdoost, M. M.; Bagherzadeh, M. Monomeric and dimeric oxido−peroxido tungsten(VI) complexes in catalytic and stoichiometric epoxidation. *Coord. Chem. Rev.* **2014**, *268*, 83−100.
(32) Arcoria, A.; Ballistreri, F. P.; Tomaselli, G. A.; Di Furia, F.; Modena, G. Opposite regioselectivity in the epoxidation of geraniol and linalool with molybdenum and tungsten peroxo complexes. *J. Org. Chem.* **1986**, *51*, 2374−2376.
(33) Mimoun, H. The role of peroxymetallation in selective oxidative processes. *J. Mol. Catal.* **1980**, *7*, 1−29.
(34) Mimoun, H.; Seree De Roch, I.; Sajus, L. Epoxydation des olefines par les complexes peroxydiques covalents du molybdene—VI. *Tetrahedron* **1970**, *26*, 37−50.
(35) Di Furia, F.; Modena, G. Mechanism of oxygen transfer from peroxo species. 1982, *54* (10), 351−351, DOI: 10.1002/bscb.19820910510.
(36) Shen, Y.; Jiang, P.; Zhang, J.; Bian, G.; Zhang, P.; Dong, Y.; Zhang, W. Highly dispersed molybdenum incorporated hollow mesoporous silica spheres as an efficient catalyst on epoxidation of olefins. *Mol. Catal.* **2017**, *433*, 212−223.
(37) Kuwahara, Y.; Furuichi, N.; Seki, H.; Yamashita, H. One-pot synthesis of molybdenum oxide nanoparticles encapsulated in hollow silica spheres: an efficient and reusable catalyst for epoxidation of olefins. *J. Mater. Chem. A* **2017**, *5*, 18518−18526.
(38) Barrio, L.; Campos-Martín, J. M.; De Frutos, M. P.; Fierro, J. L. G. Alkene Epoxidation with Ethylbenzene Hydroperoxides Using Molybdenum Heterogeneous Catalysts. *Ind. Eng. Chem. Res.* **2008**, *47*, 8016−8024.
(39) Prasetyoko, D.; Fansuri, H.; Ramli, Z.; Endud, S.; Nur, H. Tungsten Oxides-Containing Titanium Silicalite for Liquid Phase Epoxidation of 1-octene with Aqueous Hydrogen Peroxide. *Catal. Lett.* **2009**, *128*, 177−182.
(40) Gelbard, G.; Gauducheau, T.; Vidal, E.; Parvulescu, V. I.; Crosman, A.; Pop, V. M. Epoxidation with peroxotungstic acid immobilised onto silica-grafted phosphoramides. *J. Mol. Catal. A: Chem.* **2002**, *182-183*, 257−266.
(41) Maheswari, R.; Pachamuthu, M. P.; Ramanathan, A.; Subramaniam, B. Synthesis, Characterization, and Epoxidation Activity of Tungsten-Incorporated SBA-16 (W-SBA-16). *Ind. Eng. Chem. Res.* **2014**, *53*, 18833−18839.
(42) Hammond, C.; Straus, J.; Righettoni, M.; Pratsinis, S. E.; Hermans, I. Nanoparticulate Tungsten Oxide for Catalytic Epoxidations. *ACS Catal.* **2013**, *3*, 321−327.
(43) Yan, W.; Ramanathan, A.; Ghanta, M.; Subramaniam, B. Towards highly selective ethylene epoxidation catalysts using hydrogen peroxide and tungsten- or niobium-incorporated mesoporous silicate (KIT-6). *Catal. Sci. Technol.* **2014**, *4*, 4433−4439.

(44) Morales-Delarosa, S.; Campos-Martin, J. M.; Terreros, P.; Fierro, J. L. G. Catalytic Epoxidation of Cyclohexene with Tert-butylhydroperoxide Using an Immobilized Molybdenum Catalyst. *Top. Catal.* **2015**, *58*, 325−333.
(45) Mizuno, N.; Yamaguchi, K.; Kamata, K. Epoxidation of olefins with hydrogen peroxide catalyzed by polyoxometalates. *Coord. Chem. Rev.* **2005**, *249*, 1944−1956.
(46) Kurusu, Y.; Masuyama, Y.; Saito, M.; Saito, S. Epoxidation with t-butyl hydroperoxide in the presence of molybdenum peroxide and polymer-immobilized molybdenum peroxide. *J. Mol. Catal.* **1986**, *37*, 235−241.
(47) Madon, R. J.; Boudart, M. Experimental criterion for the absence of artifacts in the measurement of rates of heterogeneous catalytic reactions. *Ind. Eng. Chem. Fundam.* **1982**, *21*, 438−447.
(48) Eaton, T. R.; Boston, A. M.; Thompson, A. B.; Gray, K. A.; Notestein, J. M. Counting Active Sites on Titanium Oxide-Silica Catalysts for Hydrogen Peroxide Activation through In Situ Poisoning with Phenylphosphonic Acid. *ChemCatChem* **2014**, *6*, 3215−3222.
(49) Groves, J. T.; Nemo, T. E.; Myers, R. S. Hydroxylation and epoxidation catalyzed by iron-porphine complexes. Oxygen transfer from iodosylbenzene. *J. Am. Chem. Soc.* **1979**, *101*, 1032−1033.
(50) Tosheva, L.; Mihailova, B.; Valtchev, V.; Sterte, J. Zeolite beta spheres. *Microporous Mesoporous Mater.* **2001**, *48*, 31−37.
(51) Neelakantan, P. Raman spectrum of acetonitrile. *Proc. Indian Acad. Sci.* **1964**, *60*, 422−424.
(52) Mihailova, B.; Valtchev, V.; Mintova, S.; Faust, A. C.; Petkov, N.; Bein, T. Interlayer stacking disorder in zeolite beta family: a Raman spectroscopic study. *Phys. Chem. Chem. Phys.* **2005**, *7*, 2756.
(53) Bordiga, S.; Damin, A.; Bonino, F.; Ricchiardi, G.; Lamberti, C.; Zecchina, A. The Structure of the Peroxo Species in the TS-1 Catalyst as Investigated by Resonant Raman Spectroscopy. *Angew. Chem., Int. Ed.* **2002**, *41*, 4734−4737.
(54) Maniatakou, A.; Karaliota, S.; Mavri, M.; Raptopoulou, C.; Terzis, A.; Karaliota, A. Synthesis, characterization and crystal structure of novel mononuclear peroxotungsten(VI) complexes. Insulinomimetic activity of W(VI) and Nb(V) peroxo complexes. *J. Inorg. Biochem.* **2009**, *103*, 859−868.
(55) Zecchina, A.; Bordiga, S.; Spoto, G.; Damin, A.; Berlier, G.; Bonino, F.; Prestipino, C.; Prestipino, C. In situ characterization of catalysts active in partial oxidations: TS-1 and Fe-MFI case studies. *Top. Catal.* **2002**, *21*, 67−78.
(56) Bonino, F.; Damin, A.; Ricchiardi, G.; Ricci, M.; Spanò, G.; D'Aloisio, R.; Zecchina, A.; Lamberti, C.; Prestipino, C.; Bordiga, S. Ti-Peroxo Species in the TS-1/H2O2/H2O System. *J. Phys. Chem. B* **2004**, *108*, 3573−3583.
(57) Colomban, P. G.; Raman, G. Raman Scattering Theory and Elements of Raman Instrumentation. In *Raman Spectroscopy for Soft Matter Applications*; Amer, M. S., Ed. John Wiley & Sons, Inc.: 2009.
(58) Hu, H.; Wachs, I. E.; Bare, S. R. Surface Structures of Supported Molybdenum Oxide Catalysts: Characterization by Raman and Mo L3-Edge XANES. *J. Phys. Chem.* **1995**, *99*, 10897−10910.
(59) Ross-Medgaarden, E. I.; Wachs, I. E. Structural Determination of Bulk and Surface Tungsten Oxides with UV−vis Diffuse Reflectance Spectroscopy and Raman Spectroscopy. *J. Phys. Chem. C* **2007**, *111*, 15089−15099.
(60) Dengel, A. C.; Griffith, W. P.; Powell, R. D.; Skapski, A. C. Studies on transition-metal peroxo complexes. Part 7. Molybdenum-(VI) and tungsten(VI) carboxylato peroxo complexes, and the X-ray crystal structure of $K_2[MoO(O_2)_2(glyc)]2H_2O$. *J. Chem. Soc., Dalton Trans.* **1987**, 991.
(61) Kholdeeva, O. A. Selective Oxidations Catalyzed by Mesoporous Metal Silicates. In *Liquid Phase Oxidation via Heterogeneous Catalysis: Organic Synthesis and Industrial Applications*; Clerici, M. G. K., Kholdeeva, O. A., Ed. John Wiley & Sons, Inc.: 2013; p 127, DOI: 10.1002/9781118356760.ch4.
(62) Yoon, C. W.; Hirsekorn, K. F.; Neidig, M. L.; Yang, X.; Tilley, T. D. Mechanism of the Decomposition of Aqueous Hydrogen Peroxide over Heterogeneous TiSBA15 and TS-1 Selective Oxidation Catalysts: Insights from Spectroscopic and Density Functional Theory Studies. *ACS Catal.* **2011**, *1*, 1665−1678.
(63) Maurya, M. R.; Bharti, N. Synthesis, thermal and spectral studies of oxoperoxo and dioxo complexes of vanadium(V), molybdenum(VI) and tungsten(VI) with 2-(a-hydroxyalkyl/aryl)-benzimidazole. *Transition Met. Chem.* **1999**, *24*, 389−393.
(64) Carati, A.; Flego, C.; Previde Massara, E.; Millini, R.; Carluccio, L.; Parker, W. O., Jr.; Bellussi, G. Stability of Ti in MFI and Beta structures: a comparative study. *Microporous Mesoporous Mater.* **1999**, *30*, 137−144.
(65) Marchese, L.; Maschmeyer, T.; Gianotti, E.; Coluccia, S.; Thomas, J. M. Probing the Titanium Sites in Ti−MCM41 by Diffuse Reflectance and Photoluminescence UV−Vis Spectroscopies. *J. Phys. Chem. B* **1997**, *101*, 8836−8838.
(66) Brutchey, R. L.; Ruddy, D. A.; Andersen, L. K.; Tilley, T. D. Influence of Surface Modification of Ti−SBA15 Catalysts on the Epoxidation Mechanism for Cyclohexene with Aqueous Hydrogen Peroxide. *Langmuir* **2005**, *21*, 9576−9583.
(67) Yang, G.; Pidko, E. A.; Hensen, E. J. M. Structure, Stability, and Lewis Acidity of Mono and Double Ti, Zr, and Sn Framework Substitutions in BEA Zeolites: A Periodic Density Functional Theory Study. *J. Phys. Chem. C* **2013**, *117*, 3976−3986.
(68) Tielens, F.; Shishido, T.; Dzwigaj, S. What Do the Niobium Framework Sites Look Like in Redox Zeolites? A Combined Theoretical and Experimental Investigation. *J. Phys. Chem. C* **2010**, *114*, 3140−3147.
(69) Nogier, J.-P.; Millot, Y.; Man, P. P.; Méthivier, C.; Che, M.; Dzwigaj, S. Nature, Environment and Quantification of Titanium Species in TiSiBEA Zeolites Investigated by XRD, NMR, DR UV−Vis and XPS. *Catal. Lett.* **2009**, *130*, 588−592.
(70) Nunes, C. D.; Valente, A. A.; Pillinger, M.; Rocha, J.; Gonçalves, I. S. Molecular Structure−Activity Relationships for the Oxidation of Organic Compounds Using Mesoporous Silica Catalysts Derivatised with Bis(halogeno)dioxomolybdenum(VI) Complexes. *Chem. − Eur. J.* **2003**, *9*, 4380−4390.
(71) Morey, M. S.; Bryan, J. D.; Schwarz, S.; Stucky, G. D. Pore Surface Functionalization of MCM-48 Mesoporous Silica with Tungsten and Molybdenum Metal Centers: Perspectives on Catalytic Peroxide Activation. *Chem. Mater.* **2000**, *12*, 3435−3444.
(72) Merle, N.; Le Quéméner, F.; Barman, S.; Samantaray, M. K.; Szeto, K. C.; De Mallmann, A.; Taoufik, M.; Basset, J.-M. Well-defined silica supported bipodal molybdenum oxo alkyl complexes: a model of the active sites of industrial olefin metathesis catalysts. *Chem. Commun.* **2017**, *53*, 11338−11341.
(73) Chan, K. W.; Mance, D.; Safonova, O. V.; Copéret, C. Well-Defined Silica-Supported Tungsten(IV)−Oxo Complex: Olefin Metathesis Activity, Initiation, and Role of Brønsted Acid Sites. *J. Am. Chem. Soc.* **2019**, *141*, 18286−18292.
(74) Lwin, S.; Li, Y.; Frenkel, A. I.; Wachs, I. E. Nature of WOxSites on $SiO_2$and Their Molecular Structure−Reactivity/Selectivity Relationships for Propylene Metathesis. *ACS Catal.* **2016**, *6*, 3061−3071.
(75) Mougel, V.; Chan, K.-W.; Siddiqi, G.; Kawakita, K.; Nagae, H.; Tsurugi, H.; Mashima, K.; Safonova, O.; Copéret, C. Low Temperature Activation of Supported Metathesis Catalysts by Organosilicon Reducing Agents. *ACS Cent. Sci.* **2016**, *2*, 569−576.
(76) Skara, G.; Baran, R.; Onfroy, T.; De Proft, F.; Dzwigaj, S.; Tielens, F. Characterization of zeolitic intraframework molybdenum sites. *Microporous Mesoporous Mater.* **2016**, *225*, 355−364.
(77) Kurleto, K.; Tielens, F.; Handzlik, J. Isolated Molybdenum(VI) and Tungsten(VI) Oxide Species on Partly Dehydroxylated Silica: A Computational Perspective. *J. Phys. Chem. C* **2020**, *124*, 3002−3013.
(78) Sever, R. R.; Root, T. W. DFT Study of Solvent Coordination Effects on Titanium-Based Epoxidation Catalysts. Part Two: Reactivity of Titanium Hydroperoxo Complexes in Ethylene Epoxidation. *J. Phys. Chem. B* **2003**, *107*, 4090−4099.
(79) Crosman, A.; Gelbard, G.; Poncelet, G.; Parvulescu, V. I. Epoxidation of cyclohexene and indene with hydrogen peroxide in the presence of WO5 onto hydroxyapatite as catalyst. *Appl. Catal., A* **2004**, *264*, 23−32.

(80) Tatsumi, T.; Yamamoto, K.; Tajima, H.; Tominaga, H.-O. Shape Selective Epoxidation of Alkenes Catalyzed by Polyoxometalate-Intercalated Hydrotalcite. *Chem. Lett.* **1992**, *21*, 815−818.
(81) Cundari, T. R.; Drago, R. S. Molecular orbital investigation of ruthenium-oxo-catalyzed epoxidations. *Inorg. Chem.* **1990**, *29*, 487−493.
(82) Dobson, J. C.; Seok, W. K.; Meyer, T. J. Epoxidation and catalytic oxidation of olefins based on a RuIV:O/RuII-OH_2 couple. *Inorg. Chem.* **1986**, *25*, 1513−1514.
(83) Raj, N. K. K.; Ramaswamy, A. V.; Manikandan, P. Oxidation of norbornene over vanadium-substituted phosphomolybdic acid catalysts and spectroscopic investigations. *J. Mol. Catal. A: Chem.* **2005**, *227*, 37−45.
(84) Kuznetsov, M. L.; Pessoa, J. C. Epoxidation of olefins catalysed by vanadium−salan complexes: a theoretical mechanistic study. *Dalton Trans.* **2009**, *28*, 5460−5468.
(85) Bregante, D. T.; Tan, J. Z.; Schultz, R. L.; Ayla, E. Z.; Potts, D. S.; Torres, C.; Flaherty, D. W. Catalytic Consequences of Oxidant, Alkene, and Pore Structures on Alkene Epoxidations within Titanium Silicates. *ACS Catal.* **2020**, 10169−10184.
(86) Bregante, D. T.; Patel, A. Y.; Johnson, A. M.; Flaherty, D. W. Catalytic thiophene oxidation by groups 4 and 5 framework-substituted zeolites with hydrogen peroxide: Mechanistic and spectroscopic evidence for the effects of metal Lewis acidity and solvent Lewis basicity. *J. Catal.* **2018**, *364*, 415−425.
(87) Hammond, G. S. A Correlation of Reaction Rates. *J. Am. Chem. Soc.* **1955**, *77*, 334−338.
(88) Klein, D. R., *Organic Chemistry*. 2nd ed.; Wiley: 2013.
(89) Mulliken, R. S. A New Electroaffinity Scale; Together with Data on Valence States and on Valence Ionization Potentials and Electron Affinities. *J. Chem. Phys.* **1934**, *2*, 782.

https://dx.doi.org/10.1021/acscatal.0c03394
ACS Catal. 2021, 11, 139−154